Article:
Solyom, S., Di Benedetti, M. orcid.org/0000-0001-7870-1323 and Balázs, G.L. (2021) Bond of FRP bars in air-entrained concrete : experimental and statistical study. Construction and Building Materials, 300. 124193. ISSN 0950-0618

https://doi.org/10.1016/j.conbuildmat.2021.124193

Construction and Building Materials 300 (2021) 124193

Contents lists available at ScienceDirect

Construction and Building Materials

journal homepage: www.elsevier.com/locate/conbuildmat

Bond of FRP bars in air-entrained concrete: Experimental and statistical study

Sandor Solyom [a,*], Matteo Di Benedetti [b], György L. Balázs [a]

[a] Department of Construction Materials and Technologies, Budapest University of Technology and Economics, Muegyetem rkp 3, 1111 Budapest, Hungary
[b] Multidisciplinary Engineering Education, The University of Sheffield, The Diamond, 32 Leavygreave Road, Sheffield S3 7RD, UK

ARTICLE INFO

Keywords:
Bond
FRP
Air-entrained concrete
Statistical analysis
Pull-out test

ABSTRACT

The combined use of Fibre Reinforced Polymer (FRP) and Air-Entrained Concrete (AEC) can be an alternative to traditional steel-reinforced concrete as this system is less affected by the corrosion of the reinforcement and by the freeze-thaw cycles induced concrete degradation. However, the viability of this system hinges on the bond performance of the reinforcing bars. A total of 236 pull-out specimens were prepared and tested to study the effect of air-entraining admixtures (AEA) on the bond behaviour of FRP bars to concrete with varying compressive strengths. Failure modes and bond stress-slip curves were reported and discussed. The bond energy, calculated as the area under the bond stress-slip diagram, was also analyzed. The experimental peak bond stresses (bond strength) were compared to the theoretical ones characterized by the formula proposed for steel bars by the Model Code 2010. In addition, the statistical significance of the effect of AEA on bond characteristics was determined, yielding a reduction factor to account for the effect of AEA on bond strength. The test results show that the bond strength of FRP bars in AEC was statistically significantly lower than in normal concrete. However, the decrease is sufficiently small that could be accounted for, during the design stage, by merely increasing the reinforcement development length.

1. Introduction

Two of the main causes leading to the degradation of reinforced concrete structures are the corrosion of steel reinforcement and the concrete degradation caused by the freeze-thaw cycles [1]. Fibre Reinforced Polymer (FRP) bars are an alternative solution [2] to reduce durability related issues triggered by the corrosion of steel reinforcement. The majority of available FRP bars on the market are made from aramid (AFRP), carbon (CFRP), basalt (BFRP) or glass (GFRP) fibres. Additional to superior mechanical properties, FRP bars have a low specific weight, high corrosion resistance, electromagnetic neutrality and low life-cycle maintenance cost [3,4]. Unlike steel, FRPs exhibit linear elastic behaviour up to failure, and their elastic modulus is typically lower than that of steel. GFRP bars are the most frequently used FRP bars in the construction industry due to their lower initial cost.

Air-entrained concrete (AEC) is a particular type of concrete that was developed [5] and improved thanks to the advancements in the field of construction chemicals [6] to prevent concrete deterioration due to freeze-thaw cycles. In AEC, an artificial air void system consisting of approximately equally distributed small size pores is created in the cement paste. This allows absorbing the volumetric expansion due to the freezing water minimizing the internal damage [7,8]. While the air-entraining admixture (AEA) increases the workability of the fresh concrete [9], to ensure proper performance of the hardened AEC, controlling the air content and its stability in the concrete during casting is paramount [6,10]. The characteristics of the air voids system have been found to play a dominant role in estimating the freeze-thaw durability as they are directly linked to strains inside the material arising from the volume increase of freezing water [7].

FRP reinforced AEC appears to be a promising solution to simultaneously overcome the degradation induced by the corrosion of steel reinforcement as well as by the freeze-thaw cycles. However, to fully benefit from their advantageous properties, the composite behaviour of the two materials must be ensured. In particular, proper interaction must be mobilized between the concrete and FRP bars. There are numerous studies in the literature focusing on various factors of normal concrete (NC), such as concrete strength [11,12], type [13], cover [14] and age [15]; bar surface [16,17], diameter [18,19], spacing [20], position [21], bond length [22] and bar end condition [23]; along with the environmental [24] factors, accidental conditions [25,26,27], sustained

* Corresponding author.
E-mail address: solyom.sandor@emk.bme.hu (S. Solyom).

https://doi.org/10.1016/j.conbuildmat.2021.124193
Received 1 February 2021; Received in revised form 6 July 2021; Accepted 7 July 2021
Available online 20 July 2021

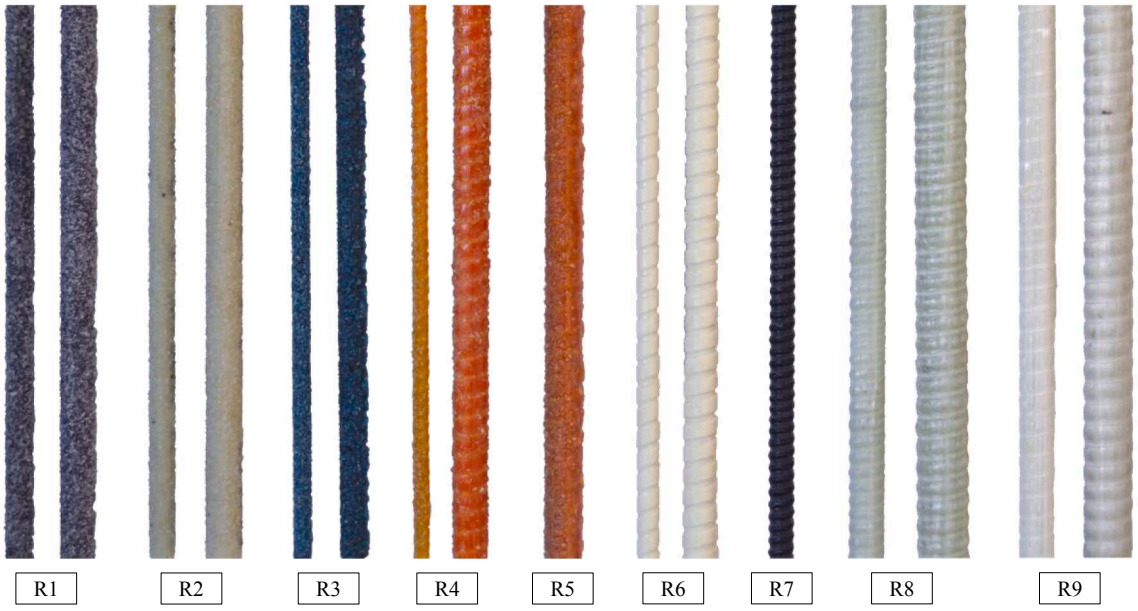

Fig. 1. FRP bars applied in the study (not each diameter is represented).

Table 1
Main physical and mechanical properties of FRP bars – as reported by the producers.

Bar symbol	Surface	Fibre	Resin	Tensile strength (MPa)	Mod. of elasticity (GPa)
R1	Sand coated (SC)	Carbon	vinyl ester	1596–1899	120–144
R2	SC	ECR Glass	vinyl ester	990–1130	50–55
R3	Helically wrapped and SC (HWSC)	HS Carbon	epoxy	> 1700	> 94
R4	HWSC	ECR Glass	epoxy	> 1100	> 50
R5	HWSC	Hybrid (C + G)	epoxy	> 1100	> 75
R6	Indented (In)	ECR Glass	vinyl ester	1500	60
R7	Ribbed (Rb)	Basalt	vinyl ester	1736	66
R8	Rb	ECR Glass	vinyl ester	> 1000	42.5
R9	Rb	ECR Glass	vinyl ester	> 1000	42.5
R10	Steel	–	–	> 500	210

Table 2
Concrete mix designs for 1 m^3 (quantities are in kg).

Symbol	Cement (CEM II/B-S 42.5 N)	Water	Sand (0-4 mm)	Coarse aggregate		Air-entraining admixture
				(4-8 mm)	(8-16 mm)	
C1	300	195	824	366	641	–
C1A	320	189	793	352	617	0.48
C2	400	160	824	366	641	–
C2A	420	155	789	351	614	0.67

stresses [28,29] and test methods [30,31]. Yet, there are no studies available on the effect of the artificially induced pores by AEA on the bond behaviour of FRP bars. Furthermore, there are only limited analyses for those of steel reinforcement [32,33].

As a result of this lack of experimental evidence, in some countries (e.

Table 3
Concrete compressive strength.

Symbol	Average	SD[a]	CV[b]
	(MPa)	(MPa)	(%)
C1	35.23	2.47	7.0
C1A	36.56	3.33	9.1
C2	76.77	8.48	11.1
C2A	72.95	7.17	9.8

[a] : Standard deviation; [b]: coefficient of variation.

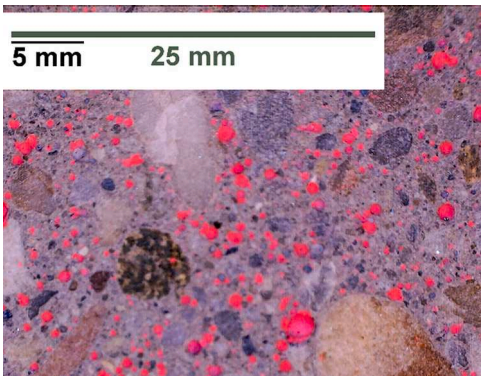

Fig. 2. Representative specimen (C2A) prepared for the determination of air void characteristics.

Table 4
Air void distribution characteristics.

Symbol	A (%)	α (mm^{-1})	$\bar{L}$(mm)
C1A	3.11	24.96	0.248
C2A	4.46	22.27	0.237

g., Hungary), AEC is precautionary not allowed to be used in bridge superstructures [34]. This is because any deterioration in bond capacity, if not properly accounted for, will impact the safety of the structure by affecting the development and transfer lengths of the reinforcement (respectively defined as the minimum embedded length demanded to develop the ultimate tensile strength of the bar [35], and as the length over which the prestressing force is totally transferred to the concrete [36]).

Mathematical statistics offer efficient methods (e.g., independent *t*-test, analysis of variance – ANOVA) to analyze whether the difference among the averages of two or more independent groups is statistically significant. Despite the evident advantages, only limited studies report statistical analysis on the bond behaviour of FRP reinforcement in concrete [37,38].

In this paper, a total of 236 centric pull-out tests were carried out to study the effect of AEA on the bond behaviour between commercially available FRP bars and different concrete compositions. Furthermore, a statistical hypothesis test was performed to infer the influence of AEA on bond characteristics and consequently estimate an appropriate reduction factor.

2. Experimental details

2.1. Materials

2.1.1. FRP bars

Fig. 1 shows the different types of FRP bars used in this study. In particular, these bars are different based on fibre type (basalt, carbon, glass and hybrid), diameter size (6 to 16 mm) and surface characteristics (sand coated (SC), sand coated with helically wrapping (HWSC), indented (In) and ribbed (Rb)). Hybrid fibre type represents a novel combination of two different fibre types (carbon and glass) to provide

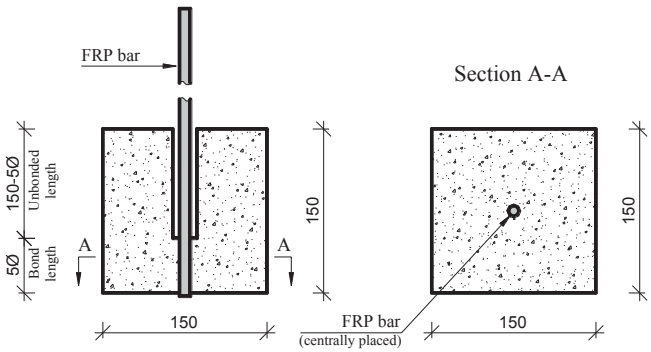

Fig. 4. Schematic representation of pull-out (P-O) test specimen (dimensions are in mm).

FRP bars with more ductile mechanical behaviour than those having only one type of fibre, as reported in [39]. Hybridization takes advantage of fibres with different elongation capacities (i.e., carbon in the inner part of the cross-section, while glass in the outer one) to obtain a pseudo-ductile tensile behaviour. The most relevant properties of the employed bars – as reported by the producers – are presented in Table 1. For comparison, traditional deformed steel bars were also tested.

2.1.2. Concrete

Four concrete mix designs (two AEC and two NC working as benchmarks) were developed for this study (Table 2). Two different concrete compressive strength levels were considered. AEC and NC mixes were designed to have an approximately equal compressive strength to minimize the effect of concrete strength on bond behaviour.

The specimens were prepared in a laboratory environment. BASF MasterGlenium 300 superplasticizer was used to set the consistency of concrete flow to class F4 [40], while Sika Air-260 was employed as the air-entraining admixture. The concrete compressive tests were carried out on three cubic specimens (150 mm) for each batch, according to EN 12390-3 [41]. The average properties of the concrete are summarised in Table 3. The relatively large coefficient of variation is justified by the fact that specimens were poured from different batches on different dates. Concrete compressive strength values for individual batches are

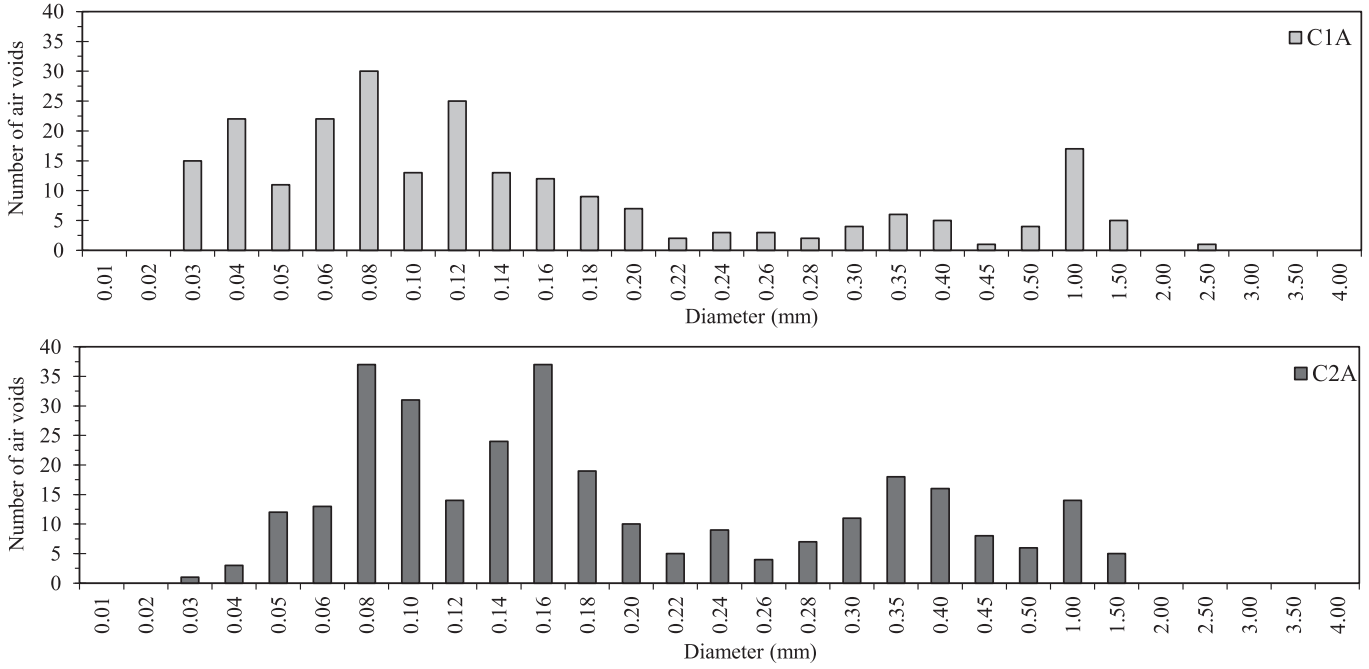

Fig. 3. Diameter distribution of the air void system.

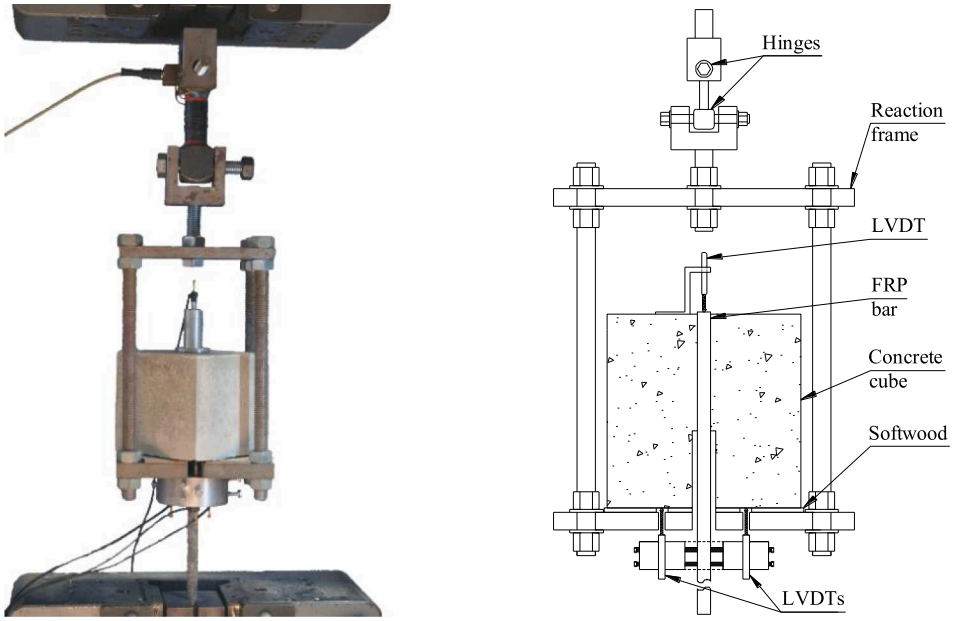

Fig. 5. Pull-out (P-O) test setup: photo and schematic representation.

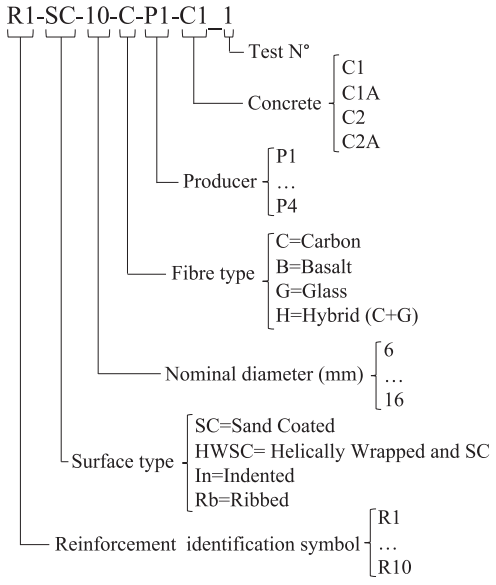

Fig. 6. Specimen symbol description.

given in the Appendix.

The performance of AEC is characterized by a set of standard parameters, such as air content (A), specific surface (α), air voids content with diameter less than 0.3 mm (A_{300}), air void diameters distribution, and spacing factor ($\bar{L}$) [42,43]. The latter is the maximum distance of any point in the cement paste from the periphery of an air void, and it is generally regarded as the most significant indicator of the cement paste matrix resistance against the exposure to freeze-thaw cycles. Not all standards currently recommend a threshold value for the spacing factor. For example, the American standard [44] sets a limit of 0.2 mm for moderate exposure, while no specific limit is given by the European standards.

Although with computational advancements, new methods have been proposed to facilitate the analysis of the air void distribution [7,45], in this paper, air void distribution was analyzed using a modified point count process as described in EN 480-11 [42]. The calculation of the spacing factor parameter assumes that air voids are evenly distributed and of uniform size and that the model has the same total volume and surface area as for the real case. However, the standard acknowledges [42] that the model is an approximation, and the value obtained is probably larger than the actual one.

The specimens used for AEC characterization are prepared based on the descriptions given in EN 480-11 [42]. However, to have a more significant representation of the AEC, pull-out specimens are cut after failure to obtain the samples for air void distribution determination. The dimensions of the prepared samples are 150 × 100 × 40 mm. To get

Table 5
Test matrix: an overview of the performed tests (✓ represents four nominally identical specimens).

	C1 and C1A concrete mixes						C2 and C2A concrete mixes					
Bar symbol	Ø6	Ø8	Ø10	Ø12	Ø14	Ø16	Ø6	Ø8	Ø10	Ø12	Ø14	Ø16
R1			✓	✓						✓		
R2	✓		✓	✓						✓		
R3	✓		✓									
R4	✓	✓	✓		✓			✓			✓	
R5					✓						✓	
R6		✓		✓				✓		✓		
R7		✓										
R8				✓		✓				✓		
R9				✓		✓				✓		
R10	✓											

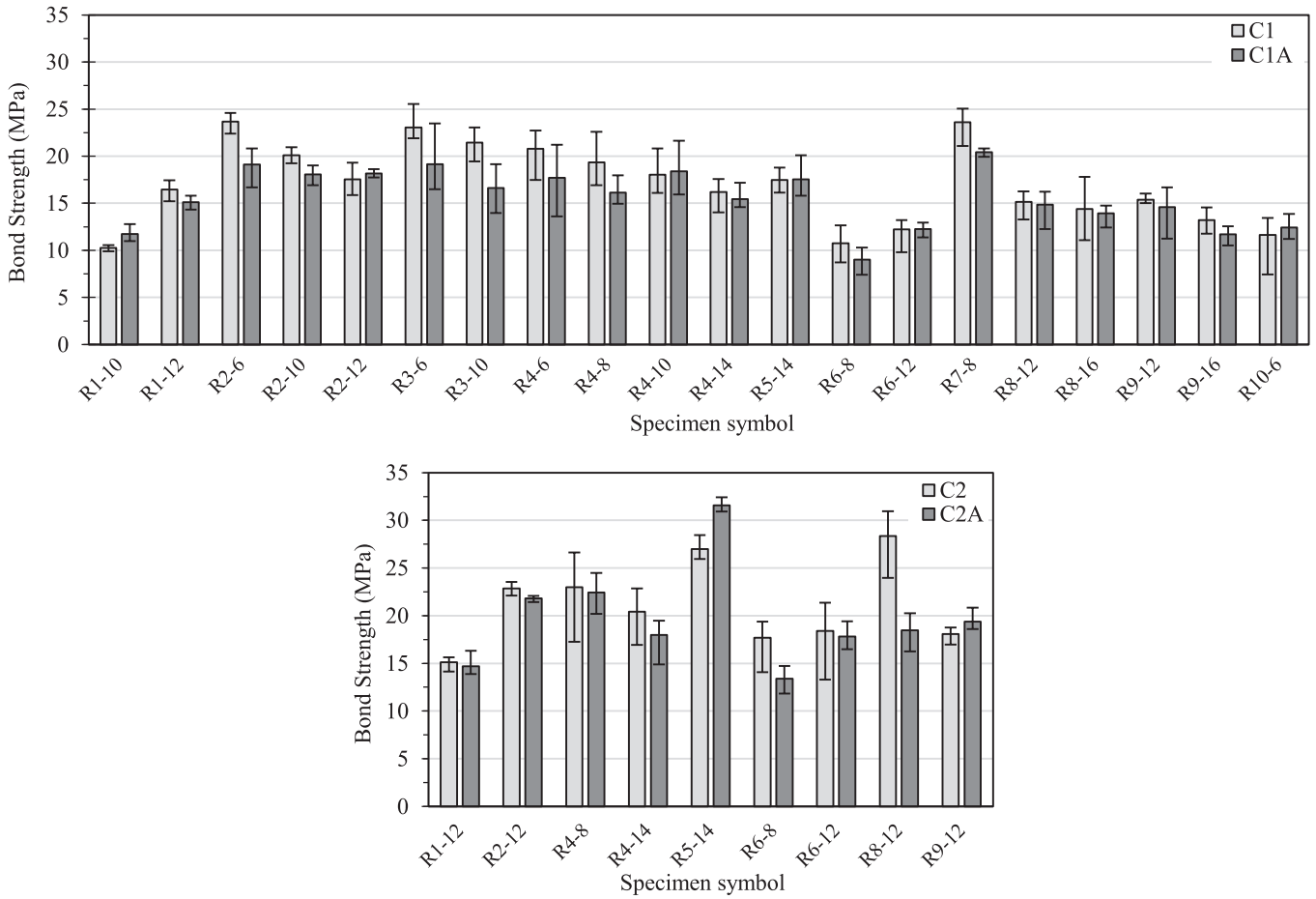

Fig. 7. Effect of AEA on bond strength in lower (top) and higher (bottom) strength concrete mixes.

meaningful results, adequate surface preparation is of paramount importance. Each specimen was ground at both sides to ensure flat, parallel surfaces. This process was followed by fine polishing (150 and 80 μm). Then specimens were oven-dried before coating with thinned lacquer for contrast enhancement of the surface.

A close-up photo of the surface of a representative specimen (C2A concrete mix) prepared for the air void characteristics definition is shown in Fig. 2, where the pink spherical parts are the air voids. Parameters for the air void microstructure characterization are shown in Table 4, while the air void diameters distribution is presented in Fig. 3 for C1A and C2A concrete, respectively. The dosage of AEA was within limits provided by the producer. The experimentally defined air void characteristics are in line with the literature (e.g., [10]), having in mind that the dosages applied in this paper belong to the lower segment of the recommended range.

2.2. Test specimens, setup and procedure

The pull-out test method was chosen to analyze the effect of different factors on the bond behaviour of FRP bars in AEC. Though this test method has some drawbacks (e.g., the stress around the concrete during the test might differ from that of during practical application [46]), it is the most widely used as it allows to effectively study the influence of different factors due to its ease of application and repeatability.

Pull-out test specimens were designed based on the recommendations of the main guidelines [47–49]. Each specimen consisted of a concrete cube of 150 mm side length [49] with an FRP bar embedded in the centre of the cube. The FRP bars were kept vertical during concrete casting. The concrete was cast in two layers, each being compacted by a vibrating table. In line with current guidelines (e.g. [47,48]), to study the local bond behaviour, the embedded length of the bar was set to 5·Ø (Ø - nominal bar diameter), which was achieved by wrapping a portion of the FRP bar with a soft insulating material to prevent bonding to the concrete. For this embedment length, the approximation of uniform shear stress can be used [48]. After casting, the specimens were left under laboratory conditions for one day, de-moulded, marked and placed underwater for six days and then removed and kept under laboratory conditions until testing. Both the pull-out and concrete characterization specimens were tested at the age of 28 days. A schematic representation of the pull-out specimen is presented in Fig. 4.

The test setup is presented in Fig. 5. The concrete pull-out specimens were placed into a custom-made metal reaction frame, and the FRP bars were gripped by the testing machine. The pull-out load was applied using a servo-hydraulic universal testing machine (Instron 5989) with a capacity of 600 kN. To capture the post-peak bond behaviour, the test was conducted at a constant crosshead displacement rate of 1 mm/min [48,49]. The gripped part of the FRP bar is considered as the loaded end (LE) of the test specimen, while the opposite is referred to as the free end (FE). Three Linear Variable Differential Transducers (LVDTs) were used to measure the relative displacement between the FRP bar and concrete at the LE, whilst one LVDT was employed at the FE. Four nominally identical specimens were tested for each configuration.

2.3. Nomenclature of tested specimens and an overview of the experimental matrix

A nomenclature is introduced to identify each specimen (Fig. 6) unequivocally. In addition, an overview of the performed experiments is presented in Table 5. Due to the commercial availability (some bars are available only in few diameter sizes) and time constraints, not all

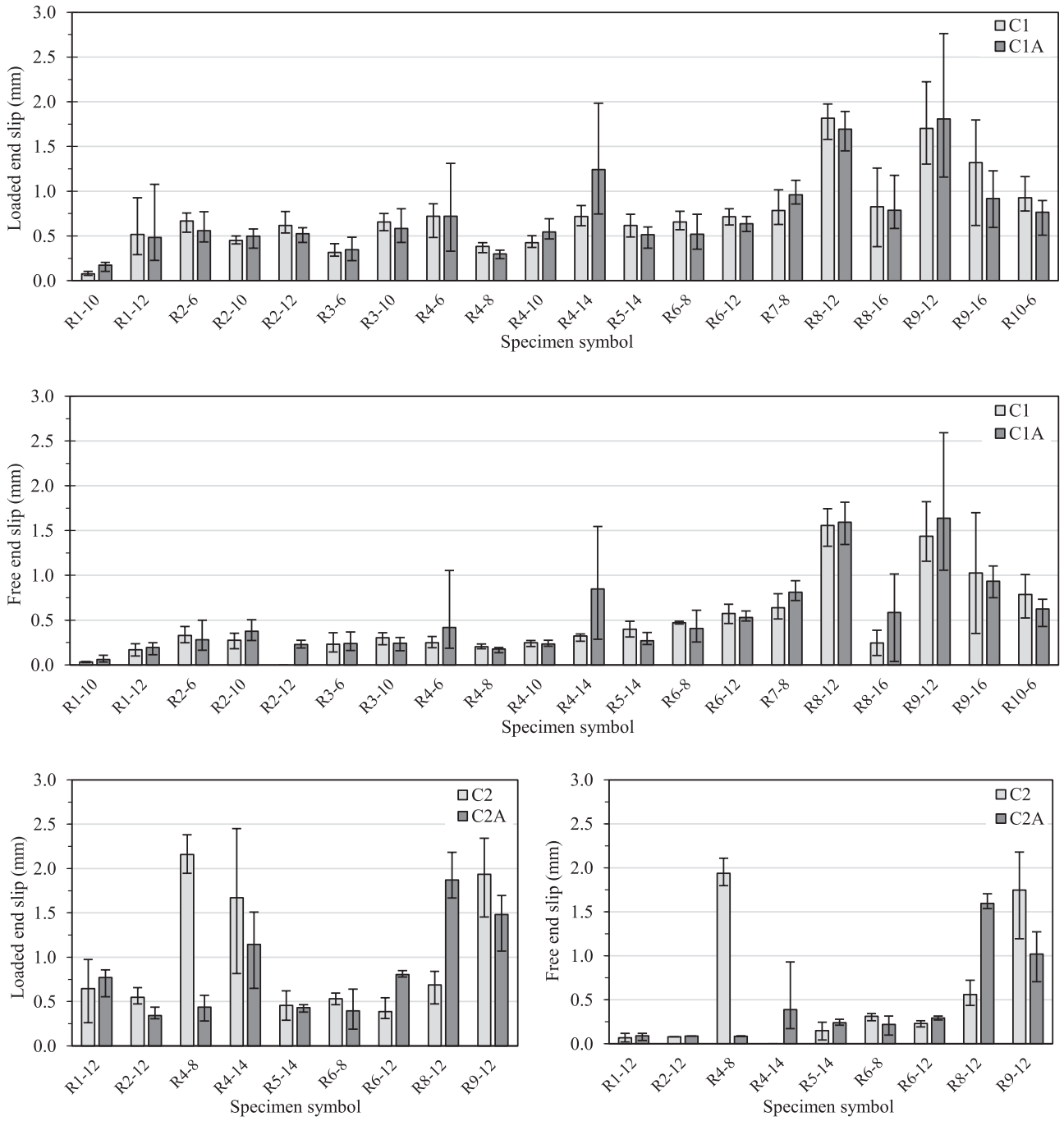

Fig. 8. Effect of AEA on LE and FE slips.

possible combinations of the considered factors were tested. It should also be noted that, for clarity, the values of the nominal diameters of bars R1 and R2 – provided by the manufacturer in the imperial unit system – are rounded to the closest nominal metric diameter in the nomenclature. However, for the calculation of specific properties (e.g., bond strength, bonded length), the provided nominal values were taken into consideration.

3. Test results and discussion

3.1. Summary of experimental results

Bond strength ($\tau_{b,max}$) was calculated by dividing the load (F_{ult}) recorded with the load cell of the testing machine by the shear surface (Eq. (1)). Uniform bond stress distribution was assumed along the bond length (l_b). The FRP bar nominal diameter is noted with the symbol $\varnothing$.

$$\tau_{b,max} = \frac{F_{ult}}{\pi \bullet \varnothing \bullet l_b} \quad (1)$$

Measurements (s) by the LVDTs attached to the loaded end of the specimen include the elastic elongation (Δl) of the portion of the bar between the embedded segment and gripping of the LVDTs, thus the loaded-end slip (s_{le}) was computed according to Eq. (2) and Eq. (3).

$$s_{le} = s - \Delta_l \quad (2)$$

$$\Delta_l = \frac{F \bullet L}{E \bullet A_b} \quad (3)$$

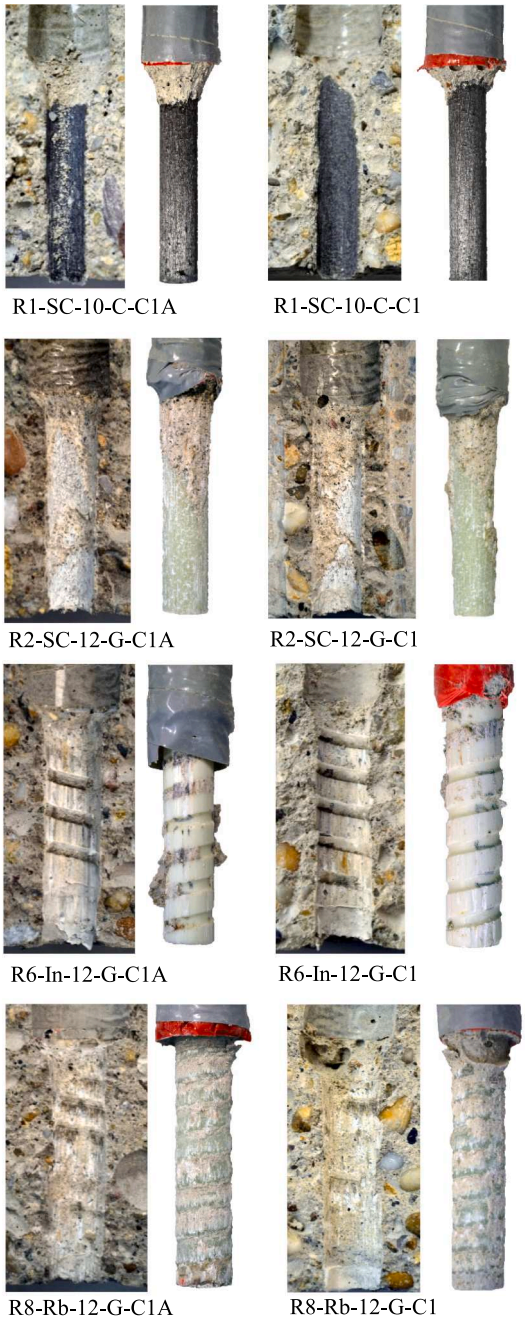

Fig. 9. Failure surfaces of representative samples of pull-out specimens (images not to scale).

Where F is the recorded load, E is the modulus of elasticity of the FRP bar, and A_b is its nominal cross-sectional area.

Measurements recorded with the LVDT attached to the free end of the specimen could be directly used as the free end slip values (s_{fe}).

As the ascending branch of the bond stress-slip curves is non-linear – especially for deformed bars – the bond strength and corresponding slip are not sufficient to accurately describe the bond behaviour. Hence, for each specimen, the bond energy (BE) was defined as the area under the ascending part of the curve, both for loaded and free end slip relationships.

Finally, bond strength results were normalized by the square root of concrete compressive strength. The mean concrete compressive strength values belonging to the standard size cylinder (150 mm in diameter, 300 mm in height) were used for normalization [50].

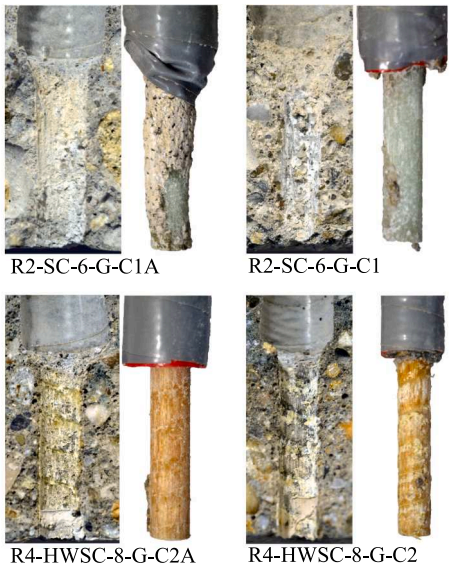

Fig. 10. Failure surfaces of R2-6 and R4-8 specimens (images not to scale).

Experimental results are tabulated in the Appendix (Table 12, 13, 14 and 15), including the bond strength ($\tau_{b,max}$, Eq. (1)), the slips at loaded ($s_{m,le}$) and free ends ($s_{m,fe}$) corresponding to the bond strength, alongside with their average values (^{a}) of nominally identical specimens, the bond energy for loaded (BE_{le}) and free end (BE_{fe}) slips, and the normalized bond strength ($\tau_{b,max}/f_{cm}^{0.5}$).

To aid the interpretation of the results, graphical illustrations are prepared in Figs. 7 and 8.

Fig. 7 shows the effect of AEA on bond strength in lower (top) and higher (bottom) strength concrete mixes. Each column represents the average value of nominally identical specimens, while the error bars (i.e., whiskers) show the range of the results. Adjacent columns represent specimens that differ only for the concrete type with NC plotted light and AEC dark. While the average bond strength for the AEC specimens tends to be lower than their NC counterparts, in most cases, the results are compatible (i.e., the range of the results partially overlap). Therefore, it is not possible to graphically infer a difference in the bond strength due to the AEA.

Similarly, the effect of AEA on LE and FE slips are presented in Fig. 8. The results for NC and AEC for lower strength concrete are consistently compatible, while, for higher strength concrete, a couple of sample types show a significant effect of AEC, namely R4-8 and R8-12. The difference in the former is attributed to the different bond stress-slip behaviour between NC and AEC samples. For the latter is assigned to the different bond stress-slip behaviour and higher concrete strength of NC specimens.

Because of the graphical compatibility of the experimental results, a statistical analysis will be necessary to determine whether the difference between NC and AEC samples (i.e., average bond strength) or lack thereof (i.e., average LE and FE slip) is significant or it is due to the inherent variability of the experimental data.

3.2. Analysis of bond failure modes

To build a coherent dataset for the statistical analysis, the failure modes of the samples are analyzed and discussed. All specimens failed by either pulling out of the bar from the concrete cube or by concrete splitting, while bar rupture and gripping failure were not observed. In particular, regardless of the concrete used, in the case of larger diameter bars (Ø16), the concrete did not provide enough confinement to avoid splitting of the cube since the embedded length of the bar reached up to 80 mm (5Ø). A similar failure mode was also recorded for about half of

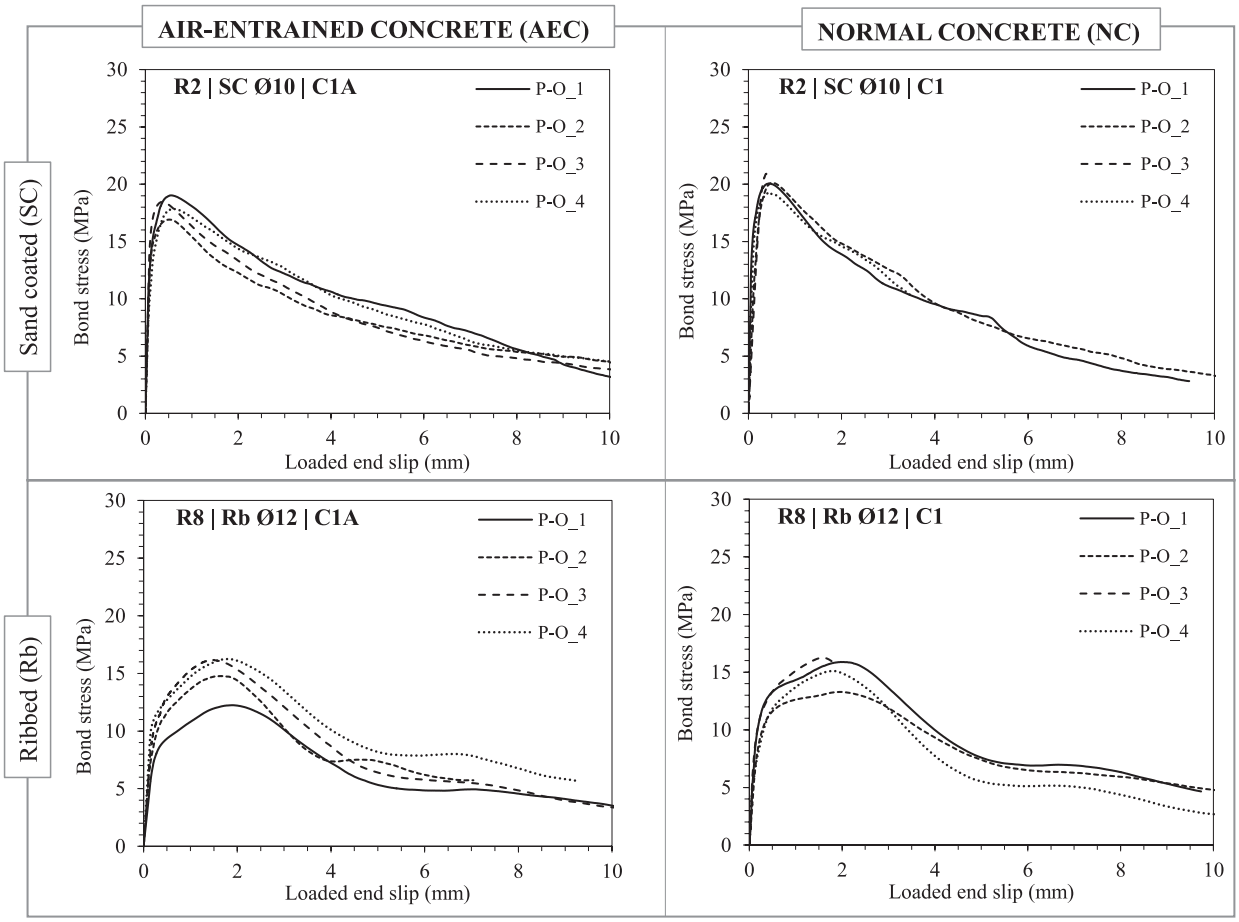

Fig. 11. Representative bond stress-slip (loaded end) relationships (the four different curves in each diagram represent four nominally identical pull-out (P-O) test results).

the specimens with 14-mm-diameter bar, conversely, all remaining samples failed by pulling out of the bar from the concrete cube. All steel bars failed by shearing off of the concrete ribs both in AEC and NC. After failure, specimens were split to closely observe the conditions of the bond failure surfaces, images of which are presented in Fig. 9 for representative AEC and NC samples. While it can be seen that, in general, the failure mode appears to be consistent for AEC and NC specimens, a couple of discrepancies were also identified (R2-6-C1 and R4-8-C2, Fig. 10).

In the case of R2-6 bars, specimens with C1A mix failed due to concrete shearing, while in those with C1 mix, the whole sand coated surface of the bar was sheared off. As the actual concrete compressive strengths are approximately equal (33 and 32 MPa, respectively for C1A and C1 mixes), the different bond failure modes could be explained by the fact that, due to entrained air, the tensile/shear resistance of concrete might be lower, thus in C1A the concrete failed before the shear capacity of the FRP surface was reached.

In the case of R4-8 bars, both for C2A and C2 concrete, the bond failure mode consisted of shearing off of the helically wrapped surface deformations and peeling off of the sand coating layer of the FRP bars. However, in the C2 mix, the FRP bar surface was more severely damaged than in C2A (Fig. 10). The lower concrete compressive strength of C2A (approximately 14%) could explain the more damaged bar surface in the case of C2 specimens.

Additional observations can be made for specific bar types. In particular, it can be seen that R1 and R2 bars failed differently (Fig. 9). The whole surface of R1 bars was always sheared off, while R2 bars failed partially within the concrete when lower strength concrete was used or by shearing off of the FRP surface in higher strength concrete. It can also be observed that the extension of the delamination for the two bars appears to be different. In the case of R1 bars, the failed surface is clean as it does not contain any concrete or sand coating debris, suggesting that the delamination occurred within the bar cross-section. However, in the case of R2 bars, the failed bar surface presents concrete and sand coating remains, furthermore the resin layer covering the fibres appears to be intact. The mechanical phenomenon leading to different delaminations is not yet understood since these bars possess the same surface characteristics, resin and fabrication process, furthermore, they are produced by the same manufacturer. This could be explained if R1 bars had higher resin content, thus making the bars more prone to interlaminar delamination; however, no analysis was carried out to support this hypostasis. This difference in the bond failure seems to have a repercussion also on the bond strength, with R1 (CFRP) bars returning values considerably lower than R2 (GFRP) bars, thus contrasting with what is reported in the literature (i.e., bond strength of CFRP equal or higher than GFRP [49,51]).

The bond energy results are summarised in the Appendix (Table 12 to Table 15); typically, a higher bond energy is associated with a more ductile behaviour. Specimens with NC and AEC show similar effects on the bond energy. As no consistent difference can be graphically determined, their effect on bond energy will be analyzed applying mathematical statistical methods in the second part of the paper.

Some additional considerations can be drawn based on the different bar surface and bond failure mode. Bars having a sand coated surface (R1 to R5) provide lower bond energy than those of deformed (R7 to R9), as they fail by shearing the sand particles off at relatively low slip values. Only R4 bars behaviour deviates from this, as these bars showed large slip values at peak bond stress. Indented bars (R6) show low bond

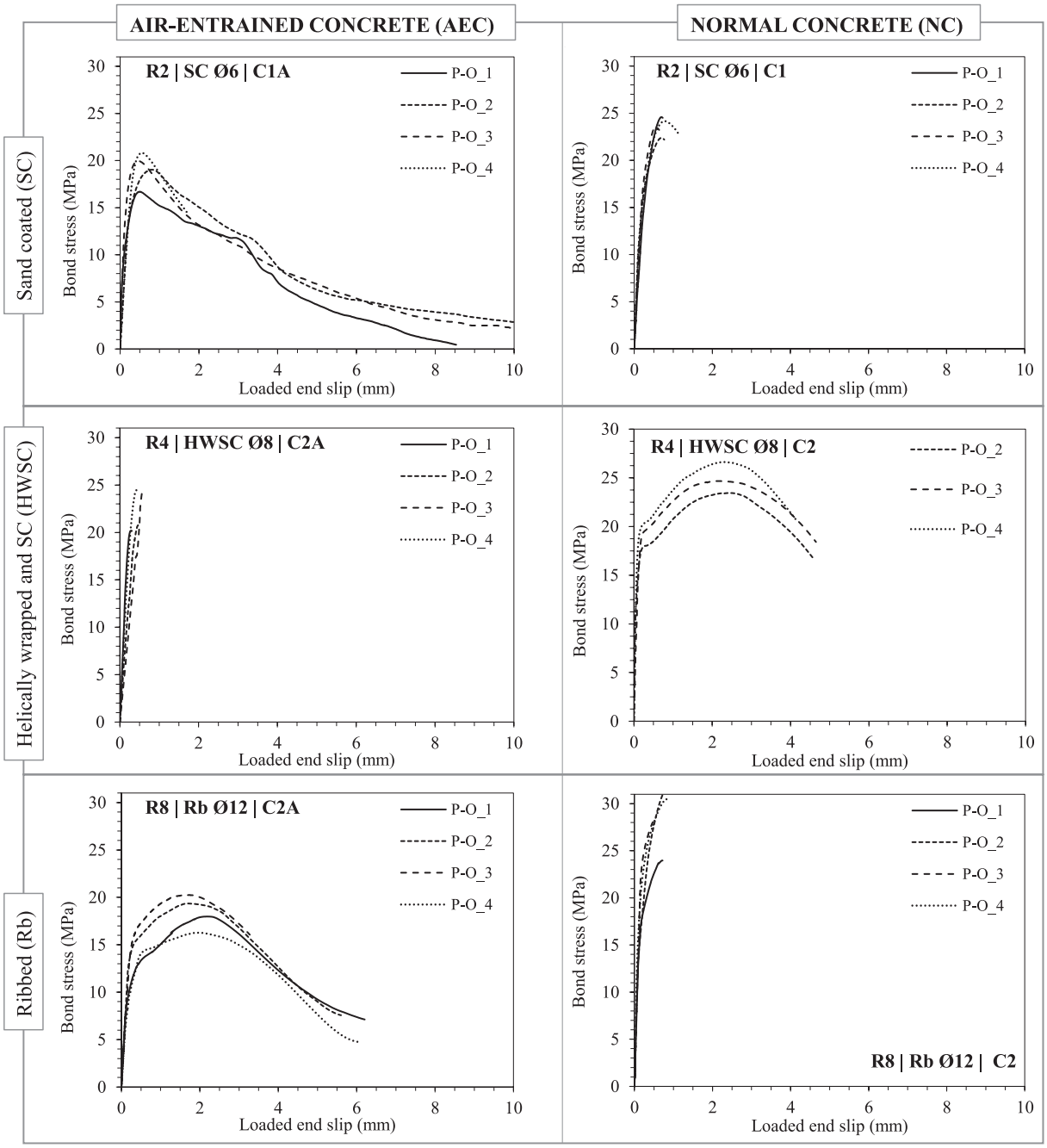

Fig. 12. Bond stress-slip (loaded end) relationships of R2-10, R4-8 and R8-12 bars (the four different curves in each diagram represent four nominally identical pull-out (P-O) test results).

energy values. Due to different surface geometry, they have relatively low bond strength values, consequently, provide low bond energy. Finally, when the failure occurs by splitting of concrete, the bond energy is lower than for a pull-out failure as the full concrete bond strength cannot be mobilized.

3.3. Bond stress–slip relationships

Fig. 11 plots the bond stress (Eq. (1)) over the LE slip (Eq. (2)). Typical curves representative of AEC (left) and NC (right) are presented. The four different curves in each diagram represent four nominally identical pull-out (P-O) test results. In general, AEA does not seem to affect the bond stress-slip relationship as the curves show similar shapes both for pre- and post-peak branches. Different parts of the bond stress-slip curves can be associated with a different bond governing mechanism (i.e., adhesion, mechanical interlock and friction). It can be concluded that AEA does not seem to affect the bond mechanisms. It can also be noted that, in the case of In and Rb deformed bars, the residual bond strength is marginally higher for NC specimens.

After careful examination of all the experimental bond stress-slip curves, only three pairs of diagrams were identified which differ between AEC and NC, namely R2-6-C1, R4-8-C2 and R8-12-C2 (Fig. 12). As it was previously presented, specimens with R2-6 bars fail due to concrete shearing in C1A concrete, while due to shearing off the sand coated layer in C1 concrete mix (Fig. 10). Failure in C1A mix is ductile due to the gradual concrete shearing, whereas the sand coating layer of the bars are sheared off suddenly, which is translated to a bond stress-slip curve that has only an ascending branch (Fig. 12). For R4-8 bars the failure

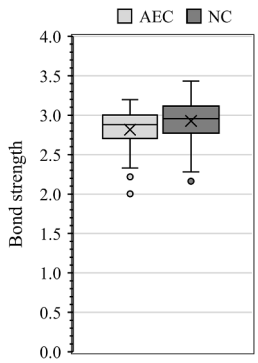

Fig. 13. Box plot diagram for the transformed database – bond strength.

Table 6
Results of the Welch *t*-test for equality of means using the transformed database: Effect of AEA on the bond strength.

t	df	p	MD	SED	95% CI	
2.560	132.516	0.012	0.110	0.043	0.025	0.194

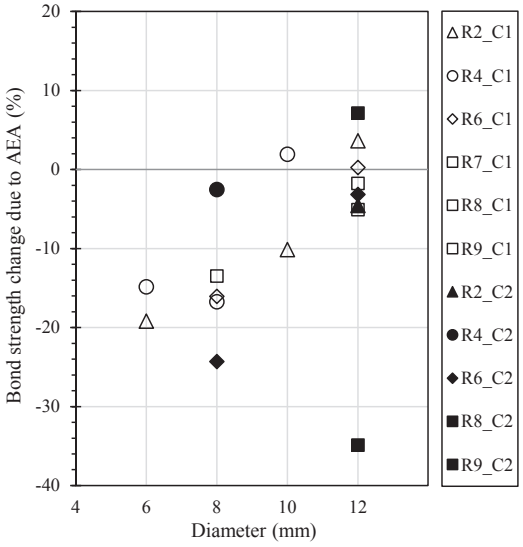

Fig. 14. Effect of air-entrainment on bond strength of different FRP bars.

Table 7
Results of the Welch *t*-test for equality of means using the transformed database: Effect of AEA on the LE slip.

	t	df	p	MD	SED	95% CI	
Sanded bars	2.733	53.483	0.008	0.310	0.113	0.082	0.537
Deformed bars	-0.664	68.990	0.509	-0.095	0.143	-0.380	0.190

Table 8
Results of the Welch *t*-test for equality of means using the transformed database: Effect of AEA on the FE slip.

	t	df	p	MD	SED	95% CI	
Sanded bars	2.039	37.962	0.048	0.415	0.204	0.003	0.828
Deformed bars	-0.216	68.633	0.830	-0.038	0.177	-0.391	0.315

Table 9
Results of the Welch *t*-test for equality of means using the transformed database: Effect of AEA on the bond energy of LE slip curves.

	t	df	p	MD	SED	95% CI	
Sanded bars	2.802	51.147	0.007	0.375	0.134	0.106	0.644
Deformed bars	0.396	66.306	0.693	0.068	0.172	-0.275	0.411

Table 10
Results of the Welch *t*-test for equality of means using the transformed database: Effect of AEA on the bond energy of FE slip curves.

	t	df	p	MD	SED	95% CI	
Sanded bars	3.187	49.493	0.002	0.818	0.257	0.302	1.334
Deformed bars	0.462	67.123	0.645	0.091	0.196	-0.301	0.483

Table 11
Results of the Welch *t*-test for equality of means using the transformed database: Effect of concrete strength in AEC and NC.

	t	df	p	MD	SED	95% CI	
AEC	3.021	59.898	0.004	0.163	0.054	0.055	0.271
NC	3.038	54.396	0.004	0.178	0.059	0.061	0.296

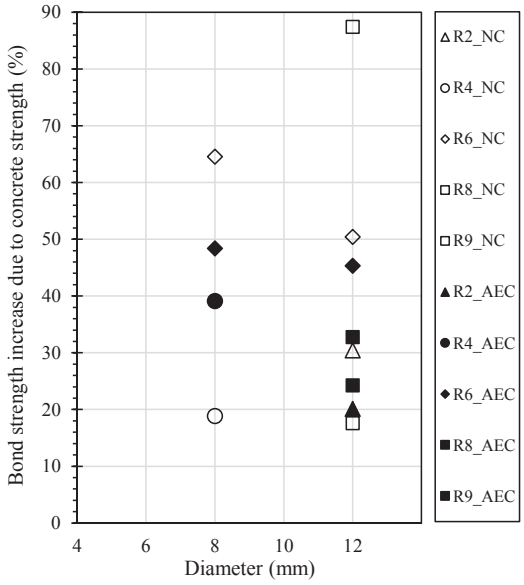

Fig. 15. Effect of concrete strength increase on bond strength.

mode was similar in C2A and C2 concrete mixes, however, FRP bar surface was more severely damaged in C2 mix that made the bond behaviour more ductile compared to that of C2A mix. Finally, as the bond failure mode for R8-12 bars was shearing off of the concrete ribs both in C2A and C2 mixes, the reason for the brittle failure of C2 may be connected to the considerably higher concrete compressive strength than for C2A (about 25%) that allowed the development of larger bond strength.

3.4. Effect of AEA on bond characteristics

Most of the experimental results describing the bond characteristics of AEC and NC specimens show partial overlapping (e.g., Fig. 7 and Fig. 8). The compatibility of the results makes it impossible to infer an evident influence of AEC on the bond parameters, even when, like in the case of the bond strength, the average values seem to suggest it exists.

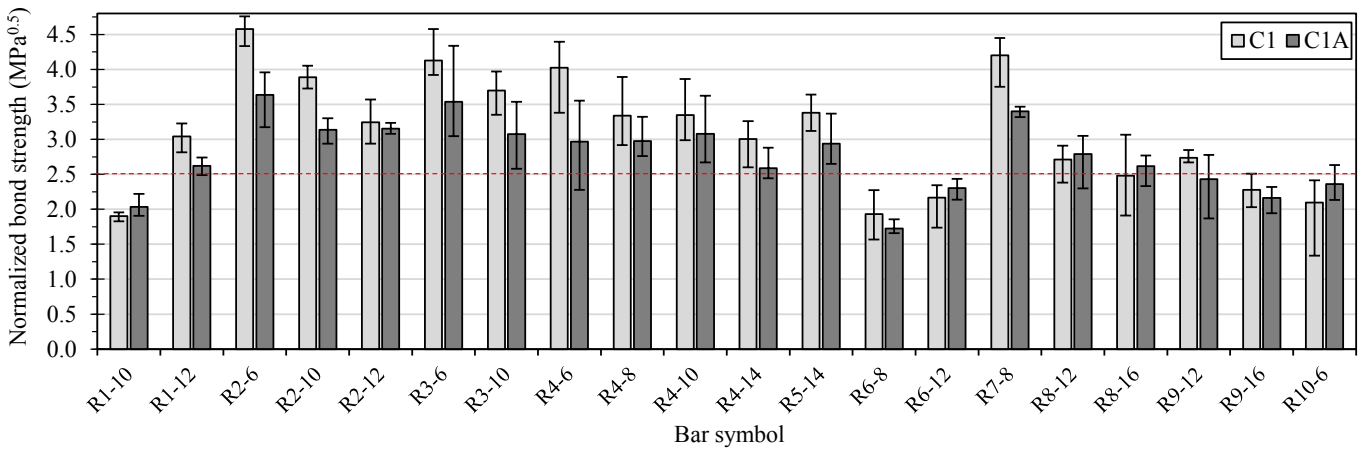

Fig. 16. Normalized bond strength in lower strength concrete mixes.

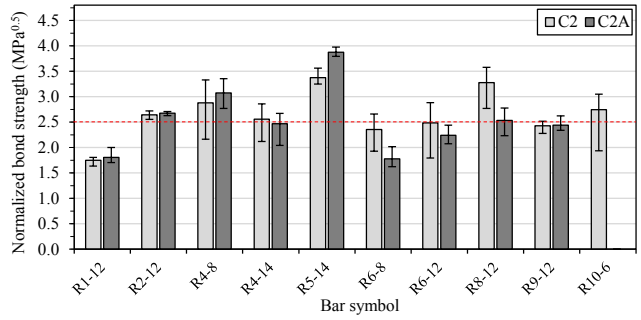

Fig. 17. Normalized bond strength in higher strength concrete mixes.

Hence, to demonstrate whether the influence of AEA is statistically significant on bond characteristics, a statistical analysis was performed.

3.4.1. Database

To create a coherent database for the statistical analysis, only those sample groups which consistently failed with the bar pulling out from the concrete were included, thus excluding all samples with 16 mm (concrete splitting failure) and 14 mm diameter bars (mixed failure mode). In addition, CFRP bars were excluded from the database because the type and strength of concrete did not influence the bond strength of R1 bars since they failed within the bar cross-section (interlaminar shear failure) rather than on the bar-concrete surface. Hence, the database prepared for statistical analysis consists of the experimental results of GFRP and BFRP bars for a total of 136 specimens. It should be noted that the database is symmetric on AEA; each experimental combination in AEC has a counterpart in NC.

3.4.2. Statistical test details

An independent-samples *t*-test can be used to ascertain if there is a difference between the sample means of two independent populations (i.e., AEC and NC) [52]. In particular, in this study, to estimate the likelihood of the means of the two independent populations being equal (null hypothesis), the Welch *t*-test [53] was run. This was selected instead of a normal independent-samples *t*-test as it is robust – to a given extent – against a possible violation of the assumption of unequal variances and mathematically more correct (the homogeneity of variances were not checked on the same database used to define the means). The significance level, indicating the probability of a false rejection of the null hypothesis in the statistical test, was chosen equal to 0.05. A p-value lower than the significance level results in the rejection of the null hypothesis and, in particular, the smaller the p-value the stronger the rejection. The statistical analysis was carried out using the IBM SPSS Statistics software v.26 [54].

To identify possible outliers, box plots were used (e.g., Fig. 13). In particular, the body of the box (i.e., box-length) represents the interquartile range (IQR), equal to the difference between 25th (Q_1) and 75th (Q_3) percentiles. Within the box, the horizontal line and the cross symbol indicate the median and the mean values, respectively. At the same time, outside, the upper and lower whiskers represent the maximum and minimum experimental values, respectively, if they are less than 1.5 times the IQR away from the edges of the body of the box, otherwise the whiskers represent 1.5 · IQR. The circle symbols are outliers. The software distinguishes two different types of extremities. Data points that are more than 1.5 box-lengths away from the edge of the box are classified as outliers, whilst those that are more than 3 box-lengths away are categorized as extreme outliers [55]. The box plot diagrams presented four outliers (two are overlapped) for the bond strength. It should be noticed that these four points are only marginally over the edge of the IQR box, thus they might have been labelled as outliers simply because of the intrinsic variability of experimental data. For this reason, it was decided not to remove them from the analysis. No extreme outlier was observed.

The distribution of the dependent variable (e.g. bond strength) in each group of the independent variable (i.e., AEC and NC) was evaluated. While a deviation from normality was observed, the groups are similarly skewed and the sample size is sufficiently large. Under such conditions, the *t*-test is known to be fairly robust to deviations from normality, thus not affecting the Type I error rate substantially [55,56].

The statistical test results will not only provide evidence if the means of the independent variable are equal, but it can also provide "how far" they are from each other. In engineering, the magnitude of such distance is not as useful as the ratio between the two means, as the latter is better suited to generalize the results (e.g., most of the available formulae for bond strength definition (e.g., [49,57,58]) take into account the effect of different parameters as a multiplicative factor). To overcome this inconvenience, it is common to mathematically manipulate the database. In particular, a transformation by natural logarithm [59], because of its algebraic properties, allows converting the difference between the means of the two samples, and the relative confidence interval, into a multiplicative factor.

3.4.3. Effect of AEA on bond strength

Table 6 shows the Welch *t*-test results for the transformed database of bond strength. In particular, *t* indicates the value of the test statistic, *df* specifies the degrees of freedom, *p* represents the statistical significance (p-value), MD denotes the mean difference that is the difference between the means of individual groups (i.e., AEC and NC). SED indicates the standard error of MD, which is the likelihood that the sample mean is accurate compared to the population mean. The smaller SED, the more likely the sample mean is close to the population mean. Finally, 95% CI

is the confidence interval of MD, which is the range of values that are believed to contain, with 95% probability, the true value of the population mean.

The p-value (0.012) lower than the set significance level allows rejecting the null hypothesis, thus inferring a statistically significant difference between the mean bond strength of NC and AEC specimens (Table 6). Mean results are 2.817 and 2.927 for AEC and NC, respectively, while the mean difference is 0.110 (95% CI of 0.025 to 0.194). Since the analysis was done on the transformed database, to obtain the statistical results for the original bond strength dataset, data were converted using the natural exponential function, resulting in a mean for the bond strength of 16.73 and 18.67 MPa, for AEC and NC, respectively, and in a ratio between the mean bond strengths of AEC and NC of 0.896 (95% CI of 0.824 to 0.976).

Hence, based on the statistical analysis, on average, approximately 10.4% of the bond strength is lost due to AEA. This can be considered as a moderate reduction of the bond strength that can be easily overcome by varying other factors (e.g., increasing the anchorage length; applying bars with different surface characteristics etc.), aiming at compensating the force transfer capacity [37]. Furthermore, based on the lower bound of the confidence interval, a conservative safety factor equal to 0.82 can be proposed to account for the bond strength loss of FRP bars due to AEA.

Influence of diameter, surface and concrete strength on the bond strength. After quantifying the overall decrease of bond strength due to AEA, the contribution of individual parameters (i.e., diameter, surface and concrete strength) is graphically studied in Fig. 14. The ordinate axis shows the bond strength change due to AEA calculated by dividing the difference between the bond strength of AEC and NC (e.g., $\tau_{b,max,C1A}$ - $\tau_{b,max,C1}$) by the bond strength of NC (e.g., $\tau_{b,max,C1}$). Negative values represent a decrease in bond strength, while positive values denote an increase. Increasing diameters are plotted on the abscissa axis. Each surface type is indicated with a different symbol, SC with a triangle, HWSC with a circle, In with a diamond, and Rb with a square. Hollow symbols represent the lower strength concrete (C1, C1A), whereas symbols for higher strength concrete (C2, C2A) are solid.

The results show a consistent trend, with the effect of AEA on the bond strength becoming less detrimental with larger diameter bars. In particular, for 12-mm-diameter bars, the difference in bond strength between AEC and NC becomes negligible. Only R8-12-C2 does not comply with this behaviour, possibly because of the difference in concrete compressive strength, which, due to different batches of concrete, was about 25% higher for C2 than C2A. In addition, while with some variability, all surface types seem to align with this trend, suggesting that the effect of AEA on the bond strength is independent of the surface type. Finally, as expected by the larger variance among the strength of the individual concrete batches (Table 3), the results for higher concrete strengths are more scattered.

3.4.4. Effect of AEA on slip

It can be observed that the slip values corresponding to the bond strength of sanded (R2 and R4) bars are considerably lower than those of deformed ones (R6 to R9) (Fig. 8). This is because different surface characteristics tend to activate differently the main bond mechanisms (adhesion, mechanical interlock and friction). As a result, to avoid an artificial increase of the scatter of the experimental data, the database was split into two groups (sanded and deformed bars), and the statistical analyses were run separately for both.

The results of the statistical analysis on the LE and FE slip are reported in Table 7 and Table 8, respectively. In both cases, because of the high p-value, the null hypothesis cannot be rejected, thus no difference can be inferred between the means for NC and AEC, for deformed bars. This implies that AEA does not statistically affect neither the LE nor the FE slip values. However, for sanded bars, the difference is statistically significant.

3.4.5. Effect of AEA on bond energy

Similarly to the slip values, the effect of AEA on the bond energy was separately analyzed for sanded and deformed bars. Results (Table 9 and Table 10) show that the effect of AEA on the bond energy is statistically significant for sanded bars only.

3.5. Effect of concrete strength on bond strength

To observe whether the concrete strength affects AEC and NC differently, another statistical analysis based on the null hypothesis test is performed.

3.5.1. Statistical analysis

To perform the statistical analysis, the transformed database was divided into two groups AEC and NC. To analyze if the effect of the concrete strength is statistically significant, the Welch *t*-test was run for both groups to determine whether the mean bond strength in lower and higher strength concrete mixes are different. Furthermore, the magnitude of the difference is estimated to compare the influence of the concrete strength on the bond strength of AEC and NC.

3.5.2. Statistical results

Table 11 shows the Welch *t*-test results for the transformed database. As the p-values (0.004 for both groups) are lower than the set significance level, the null hypothesis is rejected. Consequently, the influence of the concrete strength on the bond strength was found statistically significant for both AEC and NC specimens. The mean differences (MD) valid for the transformed database are 0.178 and 0.163 for NC and AEC, respectively. Thus, the ratios between the mean bond strengths of higher and lower concrete mixes for the original dataset are 1.195 (95% CI from 1.063 to 1.344) and 1.177 (95% CI from 1.057 to 1.311) for NC and AEC, respectively. Hence, the influence of concrete strength on the bond strength in AEC appears to be similar to that of NC, with a negligible difference of less than 2%.

3.5.3. Influence of diameter and surface type

After quantifying the overall increase of bond strength due to concrete strength in AEC and NC, the contribution of individual parameters (i.e., bar diameter and surface) is graphically studied in Fig. 15.

The abscissa axis shows increasing values of diameters, whereas on the ordinate axis there is the bond strength increase – in percentage – due to the concrete strength. This is defined by dividing the bond strength in higher strength concrete (e.g., $\tau_{b,max,C2}$) by the bond strength in lower strength concrete (e.g., $\tau_{b,max,C1}$). Each surface type is indicated with a different symbol, SC with a triangle, HWSC with a circle, In with a diamond, and Rb with a square. Solid symbols represent the AEC, while hollow ones represent the NC.

Fig. 15 shows that the beneficial effect of concrete strength on the bond strength tends to decrease with the increase of the diameter. This trend is more evident for AEC. The main outlier of this general trend is the group of R8-12 bars in NC that show the largest increase. This can be explained by the fact that the concrete compressive strength of the batch used for this group of bars was the highest among all the C2 batches. Furthermore, the surface deformation of this bar has one of the highest geometric ratios among the studied deformed bars [17] that provides this bar excellent bond capacity, thus the concrete strength increase has a more beneficial effect for this bar type.

3.5.4. Comparison to Model Code 2010

The *fib* Model Code 2010 [50] estimates the peak bond stress of a bond stress-slip relationship – for good bond condition – to be equal to 2.5 times the square root of the mean cylinder concrete compressive strength in the case of the ribbed steel bars.

To analyze the validity of this formula for FRP bars, the bond

strength was normalized by the square root of concrete strength and are plotted in Figs. 16 and 17. Furthermore, all values of normalized bond strength can be found in the Appendix alongside the experimental results. The values higher than 2.5 represent the cases where the MC2010 formula could be conservatively applied for FRP bars.

R1 bars show relatively low values that are explained by the different bond failure modes. Furthermore, indented (R6) bars present consistently lower normalized values than 2.5, while steel bars only in lower strength concrete mixes. The results for 16-mm-diameter R8 and R9 bars are marginally lower than their 12 mm counterparts, as they failed by splitting of the concrete block. In general, sanded bars possess higher values than those of deformed.

4. Conclusions

This paper presents a study on the effect of air-entraining admixtures (AEA) on the bond behaviour of FRP bars to concrete. A total of 236 pull-out specimens comprising different concrete strengths (range of compressive strength: 35 to 77 MPa), FRP bar surfaces (sand coated, sand coated with helically wrapping, indented and ribbed) and diameters (6 to 16 mm) as well as fibre types (basalt, carbon, glass and hybrid) were tested. Results are presented in terms of bond strength and corresponding loaded and free end slips (LE and FE). Bond failure modes as well as bond stress-slip relationships being analyzed. Bond energy – defined as the area under the pre-peak bond stress-slip curve – for each specimen were defined and analyzed. Furthermore, the experimentally defined bond strength values were normalized with the square root of the mean concrete compressive strength to investigate if the formulae proposed for steel bars can be applied for FRP bars as well.

Due to the inherent variance of the experimental results, graphical observation of the experimental results was assisted by mathematical statistics methods. Statistical hypothesis tests (Welch *t*-test) were run to determine if the differences in bond characteristics of AEC and normal concrete (NC) specimens were statistically significant. Because of inconsistent failure modes, bars with 14 and 16 mm diameter as well as those made with carbon fibres were excluded from the database.

Experimental results and statistical analyses led to the following conclusions.

- All BFRP and GFRP bars having a diameter between 6 and 12 mm had a consistent failure mode that is bar pulling out from the concrete. These results are used to build up the database for statistical analysis.
- AEC specimens exhibit bond failure mode and bond stress-slip behaviour similar to their NC counterparts. The few cases that differ are disclosed and discussed.
- The difference between the means of bond strength of NC and AEC is statistically significant (p-value of 0.012).
- The statistical analysis yields a ratio of the average bond strength between AEC and NC of 0.896 (95% CI of 0.824 to 0.976). That is, the mean bond strength decreases on average by approximately 10% due to the presence of AEA. A concrete-type factor should be implemented in the development length calculation to make it applicable for AEC. A preliminary conservative value of 0.82 is suggested (lower limit of CI 95%) based on the results reported herein. However, more experimental data will be required to support and generalize this value.
- As the negative influence of the AEA on the bond strength – due to entrained air – is of relatively low magnitude suggesting that FRP bars can be used in combination with AEC providing that necessary amendments are performed (e.g., considering larger development lengths).
- A consistent trend is noticeable between bond strength and the bar diameter: the effect of AEA on the bond strength is higher for lower diameter bars.
- The influence of concrete strength on the bond strength was statistically analyzed separately for AEC and NC specimens, and it was found to be significant for both groups. In particular, the ratio between the bond strength of higher and lower strength concrete mixes was 1.195 (95% CI of 1.063 to 1.344) and 1.177 (95% CI of 1.057 to 1.311) for NC and AEC, respectively. Hence, the influence of concrete strength on the bond strength in AEC appears to be similar to that of NC.
- Visual observation of the experimental data revealed that the slip values corresponding to the bond strength of sanded bars tend to be considerably lower than those of deformed. To avoid causing an artificial increase of the scatter of the experimental database, statistical analysis were run separately on the relevant sub-databases. Results showed that the effect of AEA on the slip corresponding to the bond strength is statistically significant in the case of sanded bars, yet not in the case of deformed bars. Results of the statistical analysis on the bond energies are the same as for the slips.
- The formula proposed for the peak bond stress of steel bars [50] could be conservatively applied to all tested FRP bars except those with an indented surface.

This study provides experimental and statistical evidence on the effect of AEC on the bond strength – and hence on the development length. Although a wide range of commercially available FRP bars in various concrete mixes was studied, the conclusions of this work cannot be directly applied to other types of bars and concrete. Further investigations are needed, with a similar database, to confirm the repeatability of the results and, with an augmented test matrix (e.g. applying AEA from different producers in various amounts), to generalize the conclusions and optimize the proposed reduction factor.

CRediT authorship contribution statement

Sandor Solyom: Conceptualization, Data curation, Investigation, Methodology, Formal analysis, Visualization, Writing - original draft, Writing - review & editing. **Matteo Di Benedetti:** Investigation, Methodology, Validation, Writing - review & editing. **György L. Balázs:** Funding acquisition, Supervision, Writing - review & editing.

Declaration of Competing Interest

The authors declare that they have no known competing financial interests or personal relationships that could have appeared to influence the work reported in this paper.

Acknowledgements

Authors gratefully acknowledge the financial support of the European Union by Marie Curie ITN: European Network for Durable Reinforcement and Rehabilitation Solutions (endure, Grant: PITN-GA-2013-607851) and by the NRDI Fund (TKP2020 IES, Grant No. BME-IE-WAT). Thank Assistant Professor Dr Tamás Kói for the support given for the statistical analysis. FRP bars were provided by several companies: PMB Composite, Prefa Kompozity, Pultrall Inc., Schöck Bauteile GmbH, Hughes Brothers Inc. (Fortius) and ASA.TEC, which is much appreciated.

Data availability

The data will be available upon request.

Appendix

Table 12
Experimental results for lower strength concrete mix – C1 (specimen symbols according to Fig. 6).

Specimen symbol	f_c (MPa)	$\tau_{b,max}$ (MPa)	$\tau_{b,max}$ [a] (MPa)	$s_{m,le}$ (mm)	$s_{m,le}$ [a] (mm)	$s_{m,fe}$ (mm)	$s_{m,fe}$ [a] (mm)	BE_{le} (Nmm)	BE_{le} [a] (Nmm)	BE_{fe} (Nmm)	BE_{fe} [a] (Nmm)	$\tau_{b,max}/f_{cm}^{0.5}$ ($MPa^{0.5}$)	$\tau_{b,max}/f_{cm}^{0.5}$ [a] ($MPa^{0.5}$)
R1-SC-10-C-P1-C1_1	34.20	10.39	10.27	0.104	0.076	0.029	0.032	0.70	0.64	0.29	0.29	1.92	1.90
R1-SC-10-C-P1-C1_2		9.89		0.077		0.035		0.64		0.31		1.83	
R1-SC-10-C-P1-C1_3		10.56		0.065		0.025		0.61		0.23		1.95	
R1-SC-10-C-P1-C1_4		10.25		0.058		0.038		0.60		0.35		1.90	
R1-SC-12-C-P1-C1_1	34.20	17.15	16.45	0.456	0.517	0.101	0.170	4.09	5.31	1.46	2.41	3.17	3.04
R1-SC-12-C-P1-C1_2		17.45		0.292		0.148		3.94		2.22		3.23	
R1-SC-12-C-P1-C1_3		15.98		0.393		0.195		4.62		2.74		2.96	
R1-SC-12-C-P1-C1_4		15.21		0.925		0.236		8.60		3.21		2.81	
R2-SC-6-G-P1-C1_1	31.70	24.59	23.67	0.689	0.668	0.282	0.329	11.96	11.80	6.03	6.78	4.76	4.58
R2-SC-6-G-P1-C1_2		22.39		0.685		0.359		11.87		7.13		4.33	
R2-SC-6-G-P1-C1_3		23.54		0.542		0.246		9.62		5.09		4.56	
R2-SC-6-G-P1-C1_4		24.15		0.756		0.430		13.76		8.88		4.67	
R2-SC-10-G-P1-C1_1	31.70	20.07	20.10	0.435	0.449	0.325	0.276	7.46	7.07	6.01	5.08	3.88	3.89
R2-SC-10-G-P1-C1_2		20.12		0.499		0.245		7.64		4.58		3.89	
R2-SC-10-G-P1-C1_3		20.95		0.410		0.182		5.79		3.44		4.05	
R2-SC-10-G-P1-C1_4		19.25		0.453		0.352		7.38		6.27		3.73	
R2-SC-12-G-P1-C1_1	34.20	19.30	17.53	0.772	0.616	NA	NA	10.07	7.64	0.00	-	3.57	3.24
R2-SC-12-G-P1-C1_2		16.60		0.533		NA		6.91		0.00		3.07	
R2-SC-12-G-P1-C1_3		15.88		0.544		NA		6.45		0.00		2.94	
R2-SC-12-G-P1-C1_4		18.33		0.617		NA		7.13		0.00		3.39	
R3-HWSC-6-C-P2-C1_1	36.16	22.38	23.05	0.278	0.316	0.165	0.232	4.13	5.73	3.28	4.90	4.01	4.13
R3-HWSC-6-C-P2-C1_2		25.55		0.413		0.358		8.90		8.21		4.58	
R3-HWSC-6-C-P2-C1_3		22.38		0.300		0.258		5.86		5.29		4.01	
R3-HWSC-6-C-P2-C1_4		21.89		0.273		0.146		4.03		2.81		3.92	
R3-HWSC-10-C-P2-C1_1	38.64	22.24	21.45	0.651	0.657	0.354	0.302	11.10	9.94	7.05	5.83	3.83	3.70
R3-HWSC-10-C-P2-C1_2		19.44		0.752		0.360		10.17		6.21		3.35	
R3-HWSC-10-C-P2-C1_3		21.07		0.559		0.270		8.27		5.17		3.63	
R3-HWSC-10-C-P2-C1_4		23.04		0.667		0.225		10.23		4.90		3.97	
R4-HWSC-6-G-P2-C1_1	31.70	21.58	20.79	0.482	0.720	0.192	0.247	7.39	10.19	3.80	4.61	4.18	4.02
R4-HWSC-6-G-P2-C1_2		17.46		0.799		0.316		9.94		5.04		3.38	
R4-HWSC-6-G-P2-C1_3		21.40		0.739		0.273		10.14		5.19		4.14	
R4-HWSC-6-G-P2-C1_4		22.71		0.859		0.207		13.31		4.43		4.40	
R4-HWSC-8-G-P2-C1_1	38.64	18.51	19.36	0.312	0.382	0.179	0.203	4.76	5.49	3.05	2.67	3.19	3.34
R4-HWSC-8-G-P2-C1_2		16.91		0.367		0.235		4.81		3.66		2.92	
R4-HWSC-8-G-P2-C1_3		22.58		0.423		0.194		6.08		3.99		3.89	
R4-HWSC-8-G-P2-C1_4		19.42		0.425		NA		6.31		0.00		3.35	
R4-HWSC-10-G-P2-C1_1	34.04	20.83	18.03	0.430	0.425	0.271	0.248	7.16	6.12	5.18	4.11	3.87	3.35
R4-HWSC-10-G-P2-C1_2		17.12		0.371		0.244		4.93		3.71		3.18	
R4-HWSC-10-G-P2-C1_3		18.08		0.503		0.272		7.07		4.49		3.36	
R4-HWSC-10-G-P2-C1_4		16.10		0.396		0.205		5.31		3.06		2.99	
R4-HWSC-14-G-P2-C1_1	34.04	14.02	16.20	0.724	0.717	0.341	0.322	7.56	8.95	4.41	4.74	2.60	3.01
R4-HWSC-14-G-P2-C1_2		17.58		0.840		0.264		10.61		4.24		3.26	
R4-HWSC-14-G-P2-C1_3		15.87		0.687		0.344		8.77		4.98		2.95	
R4-HWSC-14-G-P2-C1_4		17.34		0.615		0.338		8.86		5.31		3.22	
R5-HWSC-14-H-P2-C1_1	31.70	18.80	17.46	0.743	0.617	0.388	0.400	11.23	8.97	6.66	6.38	3.64	3.38
R5-HWSC-14-H-P2-C1_2		16.98		0.487		0.412		7.52		6.36		3.29	
R5-HWSC-14-H-P2-C1_3		17.95		0.734		0.488		10.67		7.95		3.47	
R5-HWSC-14-H-P2-C1_4		16.12		0.505		0.312		6.45		4.56		3.12	
R6-In-8-G-P3-C1_1	35.96	NA	10.75	NA	0.657	NA	0.470	-	5.64	-	4.41	NA	1.93
R6-In-8-G-P3-C1_2		10.89		0.568		0.457		4.87		4.16		1.96	
R6-In-8-G-P3-C1_3		12.66		0.626		0.488		7.10		5.87		2.27	
R6-In-8-G-P3-C1_4		8.71		0.777		0.465		4.94		3.20		1.57	
R6-In-12-G-P3-C1_1	36.83	12.91	12.23	0.792	0.714	0.652	0.574	8.81	7.20	7.25	5.96	2.29	2.17
R6-In-12-G-P3-C1_2		12.99		0.623		0.462		6.67		5.37		2.30	
R6-In-12-G-P3-C1_3		13.22		0.636		0.506		6.85		5.65		2.34	
R6-In-12-G-P3-C1_4		9.80		0.803		0.677		6.48		5.56		1.74	
R7-Rb-8-B-P4-C1_1	36.62	24.52	23.62	1.017	0.784	0.795	0.639	20.49	15.30	16.74	12.64	4.36	4.20
R7-Rb-8-B-P4-C1_2		21.09		0.679		0.620		12.10		10.52		3.75	
R7-Rb-8-B-P4-C1_3		25.03		0.814		0.629		16.17		13.23		4.45	
R7-Rb-8-B-P4-C1_4		23.83		0.627		0.512		12.43		10.08		4.24	
R8-Rb-12-G-P4-C1_1	36.16	15.88	15.13	1.975	1.817	1.745	1.556	26.78	23.15	24.46	20.67	2.85	2.71
R8-Rb-12-G-P4-C1_2		13.28		1.934		1.697		22.43		20.54		2.38	
R8-Rb-12-G-P4-C1_3		16.25		1.578		1.324		21.32		18.58		2.91	
R8-Rb-12-G-P4-C1_4		15.11		1.779		1.458		22.05		19.10		2.71	
R8-Rb-16-G-P4-C1_1	38.64	17.79	14.40	1.260	0.825	NA	0.246	14.26	8.13	-	2.78	3.07	2.48
R8-Rb-16-G-P4-C1_2		11.09		0.380		0.105		2.56		0.96		1.91	
R8-Rb-16-G-P4-C1_3		14.57		0.708		0.386		7.19		4.61		2.51	
R8-Rb-16-G-P4-C1_4		14.14		0.952		NA		8.51		-		2.44	
R9-Rb-12-G-P4-C1_1	36.62	15.29	15.38	1.474	1.703	1.307	1.438	17.26	20.58	16.56	18.68	2.72	2.74

(*continued on next page*)

Table 12 (*continued*)

Specimen symbol	f_c (MPa)	$\tau_{b,max}$ (MPa)	$\tau_{b,max}$ [a] (MPa)	$s_{m,le}$ (mm)	$s_{m,le}$ [a] (mm)	$s_{m,fe}$ (mm)	$s_{m,fe}$ [a] (mm)	BE_{le} (Nmm)	BE_{le} [a] (Nmm)	BE_{fe} (Nmm)	BE_{fe} [a] (Nmm)	$\tau_{b,max}/f_{cm}^{0.5}$ ($MPa^{0.5}$)	$\tau_{b,max}/f_{cm}^{0.5}$ [a] ($MPa^{0.5}$)
R9-Rb-12-G-P4-C1_2		15.21		2.224		1.822		27.77		24.28		2.70	
R9-Rb-12-G-P4-C1_3		15.01		1.811		1.462		21.20		18.63		2.67	
R9-Rb-12-G-P4-C1_4		16.02		1.303		1.159		16.11		15.23		2.85	
R9-Rb-16-G-P4-C1_1	38.64	13.27	13.21	1.396	1.319	1.004	1.028	14.61	15.05	12.03	12.43	2.29	2.28
R9-Rb-16-G-P4-C1_2		14.54		1.797		1.699		24.43		22.39		2.51	
R9-Rb-16-G-P4-C1_3		11.77		0.616		0.350		5.21		3.39		2.03	
R9-Rb-16-G-P4-C1_4		13.26		1.468		1.058		15.97		11.90		2.29	
R10-Rb-6-Steel-C1_1	35.96	12.42	11.65	1.165	0.928	1.009	0.786	12.46	8.76	10.740	7.78	2.23	2.09
R10-Rb-6-Steel-C1_2		13.34		0.910		0.796		9.57		8.340		2.40	
R10-Rb-6-Steel-C1_3		7.43		0.779		0.524		4.82		3.286		1.34	
R10-Rb-6-Steel-C1_4		13.43		0.857		0.813		8.19		8.736		2.41	

[a]Average value of nominally identical specimens; NA = not available.

Table 13
Experimental results for lower strength concrete mix – C1A (specimen symbols according to Fig. 6).

Specimen symbol	f_c (MPa)	$\tau_{b,max}$ (MPa)	$\tau_{b,max}$ [a] (MPa)	$s_{m,le}$ (mm)	$s_{m,le}$ [a] (mm)	$s_{m,fe}$ (mm)	$s_{m,fe}$ [a] (mm)	BE_{le} (Nmm)	BE_{le} [a] (Nmm)	BE_{fe} (Nmm)	BE_{fe} [a] (Nmm)	$\tau_{b,max}/f_{cm}^{0.5}$ ($MPa^{0.5}$)	$\tau_{b,max}/f_{cm}^{0.5}$ [a] ($MPa^{0.5}$)
R1-SC-10-C-P1-C1A_1	38.18	11.18	11.72	0.103	0.173	0.032	0.062	0.83	1.44	0.313	0.78	1.94	2.03
R1-SC-10-C-P1-C1A_2		11.94		0.203		0.109		1.88		1.219		2.07	
R1-SC-10-C-P1-C1A_3		10.98		0.181		0.035		1.32		NA		1.91	
R1-SC-10-C-P1-C1A_4		12.78		0.204		0.071		1.74		0.820		2.22	
R1-SC-12-C-P1-C1A_1	38.18	15.79	15.10	1.076	0.482	0.249	0.195	10.99	5.22	3.557	2.64	2.74	2.62
R1-SC-12-C-P1-C1A_2		15.72		0.227		0.114		2.81		1.626		2.73	
R1-SC-12-C-P1-C1A_3		14.33		0.329		0.176		3.63		2.248		2.49	
R1-SC-12-C-P1-C1A_4		14.56		0.297		0.241		3.44		3.111		2.53	
R2-SC-6-G-P1-C1A_1	32.66	16.70	19.12	0.489	0.560	0.252	0.282	6.53	8.32	3.765	4.88	3.18	3.64
R2-SC-6-G-P1-C1A_2		19.02		0.770		0.498		11.30		8.570		3.62	
R2-SC-6-G-P1-C1A_3		19.96		0.434		0.215		7.27		3.924		3.80	
R2-SC-6-G-P1-C1A_4		20.82		0.546		0.164		8.16		3.260		3.96	
R2-SC-10-G-P1-C1A_1	38.18	19.03	18.06	0.545	0.497	0.386	0.376	8.60	7.40	6.727	5.57	3.30	3.14
R2-SC-10-G-P1-C1A_2		16.92		0.503		0.341		7.08		5.347		2.94	
R2-SC-10-G-P1-C1A_3		18.46		0.364		0.273		5.48		4.645		3.20	
R2-SC-10-G-P1-C1A_4		17.85		0.577		0.505		8.43		NA		3.10	
R2-SC-12-G-P1-C1A_1	38.18	17.73	18.16	0.502	0.525	0.188	0.229	6.47	7.27	3.061	3.93	3.08	3.15
R2-SC-12-G-P1-C1A_2		18.10		0.582		0.276		8.06		4.495		3.14	
R2-SC-12-G-P1-C1A_3		18.63		0.426		0.202		6.35		NA		3.23	
R2-SC-12-G-P1-C1A_4		18.18		0.591		0.251		8.19		4.236		3.16	
R3-HWSC-6-C-P2-C1A_1	34.29	19.94	19.14	0.224	0.347	0.161	0.239	3.70	5.01	2.891	3.86	3.68	3.54
R3-HWSC-6-C-P2-C1A_2		23.48		0.295		0.223		5.63		4.528		4.34	
R3-HWSC-6-C-P2-C1A_3		16.66		0.485		0.369		6.16		5.080		3.08	
R3-HWSC-6-C-P2-C1A_4		16.48		0.384		0.203		4.53		2.922		3.04	
R3-HWSC-10-C-P2-C1A_1	34.29	13.96	16.63	0.436	0.584	0.245	0.242	4.63	6.40	3.132	3.66	2.58	3.07
R3-HWSC-10-C-P2-C1A_2		19.15		0.667		0.259		6.89		4.477		3.54	
R3-HWSC-10-C-P2-C1A_3		16.59		0.805		0.306		9.43		4.590		3.06	
R3-HWSC-10-C-P2-C1A_4		16.82		0.427		0.158		4.66		2.451		3.11	
R4-HWSC-6-G-P2-C1A_1	40.61	21.21	17.70	1.312	0.720	1.055	0.417	24.49	11.06	21.141	7.55	3.55	2.97
R4-HWSC-6-G-P2-C1A_2		20.91		0.713		0.185		10.27		3.542		3.50	
R4-HWSC-6-G-P2-C1A_3		13.59		0.329		0.237		3.80		2.922		2.28	
R4-HWSC-6-G-P2-C1A_4		15.09		0.527		0.191		5.66		2.606		2.53	
R4-HWSC-8-G-P2-C1A_1	34.29	14.95	16.12	0.336	0.299	0.191	0.178	4.19	3.91	2.603	2.61	2.76	2.98
R4-HWSC-8-G-P2-C1A_2		15.57		0.247		0.136		2.86		1.965		2.88	
R4-HWSC-8-G-P2-C1A_3		17.98		0.270		0.188		4.21		3.111		3.32	
R4-HWSC-8-G-P2-C1A_4		15.96		0.342		0.195		4.39		2.753		2.95	
R4-HWSC-10-G-P2-C1A_1	40.61	15.94	18.38	0.514	0.544	0.209	0.234	6.53	8.01	3.082	4.35	2.67	3.08
R4-HWSC-10-G-P2-C1A_2		21.62		0.466		0.244		8.39		4.853		3.62	
R4-HWSC-10-G-P2-C1A_3		16.81		0.693		0.209		8.99		4.565		2.82	
R4-HWSC-10-G-P2-C1A_4		19.15		0.503		0.276		8.14		4.908		3.21	
R4-HWSC-14-G-P2-C1A_1	40.61	15.01	15.45	1.355	1.241	1.045	0.847	17.57	15.74	14.449	11.89	2.52	2.59
R4-HWSC-14-G-P2-C1A_2		14.58		1.984		1.545		25.55		21.336		2.44	
R4-HWSC-14-G-P2-C1A_3		17.19		0.746		0.286		8.86		4.565		2.88	
R4-HWSC-14-G-P2-C1A_4		15.02		0.877		0.512		10.99		7.193		2.52	
R5-HWSC-14-H-P2-C1A_1	40.61	17.10	17.55	0.547	0.513	0.363	0.269	7.68	6.81	5.803	4.37	2.87	2.94
R5-HWSC-14-H-P2-C1A_2		17.18		0.599		0.251		7.18		3.974		2.88	
R5-HWSC-14-H-P2-C1A_3		15.81		0.364		0.236		4.68		3.479		2.65	
R5-HWSC-14-H-P2-C1A_4		20.09		0.542		0.227		7.71		4.220		3.37	
R6-In-8-G-P3-C1A_1	35.74	7.42	9.03	0.419	0.521	0.298	0.406	2.54	4.26	1.968	3.71	NA	1.72
R6-In-8-G-P3-C1A_2		9.20		0.569		0.462		4.29		3.666		1.66	
R6-In-8-G-P3-C1A_3		9.20		0.351		0.255		2.43		2.062		1.66	
R6-In-8-G-P3-C1A_4		10.28		0.743		0.611		6.07		5.394		1.85	
R6-In-12-G-P3-C1A_1	33.35	12.96	12.26	0.635	0.638	0.489	0.529	6.63	6.34	5.418	5.49	2.43	2.30
R6-In-12-G-P3-C1A_2		11.78		0.551		0.505		5.36		5.091		2.21	

(*continued on next page*)

Table 13 (*continued*)

Specimen symbol	f_c (MPa)	$\tau_{b,max}$ (MPa)	$\tau_{b,max}$ [a] (MPa)	$s_{m,le}$ (mm)	$s_{m,le}$ [a] (mm)	$s_{m,fe}$ (mm)	$s_{m,fe}$ [a] (mm)	BE_{le} (Nmm)	BE_{le} [a] (Nmm)	BE_{fe} (Nmm)	BE_{fe} [a] (Nmm)	$\tau_{b,max}/f_{cm}^{0.5}$ ($MPa^{0.5}$)	$\tau_{b,max}/f_{cm}^{0.5}$ [a] ($MPa^{0.5}$)
R6-In-12-G-P3-C1A_3		11.38		0.716		0.602		6.46		5.803		2.14	
R6-In-12-G-P3-C1A_4		12.93		0.649		0.518		6.90		5.653		2.43	
R7-Rb-8-B-P4-C1A_1	41.11	20.83	20.43	0.857	0.960	0.720	0.811	14.81	16.10	12.792	14.18	3.47	3.40
R7-Rb-8-B-P4-C1A_2		19.93		0.992		0.833		15.99		14.017		3.32	
R7-Rb-8-B-P4-C1A_3		20.49		0.870		0.750		13.88		12.880		3.41	
R7-Rb-8-B-P4-C1A_4		20.49		1.121		0.940		19.72		17.024		3.41	
R8-Rb-12-G-P4-C1A_1	33.35	12.25	14.86	1.891	1.693	1.817	1.593	18.82	20.42	18.891	20.05	2.30	2.79
R8-Rb-12-G-P4-C1A_2		14.78		1.654		1.513		19.94		19.164		2.78	
R8-Rb-12-G-P4-C1A_3		16.18		1.450		1.344		19.00		18.549		3.04	
R8-Rb-12-G-P4-C1A_4		16.24		1.774		1.699		23.93		23.597		3.05	
R8-Rb-16-G-P4-C1A_1	33.35	14.75	13.92	0.631	0.786	0.589	0.584	7.25	8.18	6.924	6.37	2.77	2.61
R8-Rb-16-G-P4-C1A_2		14.62		1.178		1.016		11.97		11.443		2.75	
R8-Rb-16-G-P4-C1A_3		12.42		0.753		0.693		6.83		6.589		2.33	
R8-Rb-16-G-P4-C1A_4		13.89		0.583		0.039		6.67		0.531		2.61	
R9-Rb-12-G-P4-C1A_1	41.11	16.69	14.60	1.427	1.807	1.371	1.638	18.71	19.89	18.617	18.69	2.78	2.43
R9-Rb-12-G-P4-C1A_2		14.95		1.158		1.057		13.14		12.508		2.49	
R9-Rb-12-G-P4-C1A_3		15.53		1.881		1.531		21.73		18.990		2.58	
R9-Rb-12-G-P4-C1A_4		11.24		2.762		2.592		25.97		24.657		1.87	
R9-Rb-16-G-P4-C1A_1	34.29	12.56	11.71	0.814	0.917	0.750	0.936	8.27	8.89	8.074	8.50	2.32	2.16
R9-Rb-16-G-P4-C1A_2		11.31		1.227		1.104		11.76		10.847		2.09	
R9-Rb-16-G-P4-C1A_3		12.45		1.034		0.944		10.56		9.873		2.30	
R9-Rb-16-G-P4-C1A_4		10.52		0.594		0.944		4.97		5.201		1.94	
R10-Rb-6-Steel-C1A_1	32.66	12.68	12.41	0.507	0.765	0.430	0.623	5.13	7.74	4.710	6.68	2.41	2.36
R10-Rb-6-Steel-C1A_2		13.85		0.885		0.658		9.63		7.667		2.63	
R10-Rb-6-Steel-C1A_3		11.23		0.896		0.733		8.45		7.504		2.13	
R10-Rb-6-Steel-C1A_4		11.88		0.771		0.672		7.73		6.855		2.26	

[a]Average value of nominally identical specimens; NA = not available.

Table 14
Experimental results for higher strength concrete mix – C2 (specimen symbols according to Fig. 6).

Specimen symbol	f_c (MPa)	$\tau_{b,max}$ (MPa)	$\tau_{b,max}$ [a] (MPa)	$s_{m,le}$ (mm)	$s_{m,le}$ [a] (mm)	$s_{m,fe}$ (mm)	$s_{m,fe}$ [a] (mm)	BE_{le} (Nmm)	BE_{le} [a] (Nmm)	BE_{fe} (Nmm)	BE_{fe} [a] (Nmm)	$\tau_{b,max}/f_{cm}^{0.5}$ ($MPa^{0.5}$)	$\tau_{b,max}/f_{cm}^{0.5}$ [a] ($MPa^{0.5}$)
R1-SC-12-C-P1-C2_1	86.89	14.14	15.12	0.900	0.65	0.119	0.07	7.37	5.85	1.60	1.51	1.63	1.75
R1-SC-12-C-P1-C2_2		15.26		0.976		0.099		8.75		1.42		1.76	
R1-SC-12-C-P1-C2_3		15.45		0.453		0.022		4.13		-		1.79	
R1-SC-12-C-P1-C2_4		15.63		0.260		0.029		3.17		-		1.81	
R2-SC-12-G-P1-C2_1	86.89	23.31	22.85	0.657	0.55	0.079	0.08	9.66	8.56	1.70	1.70	2.69	2.64
R2-SC-12-G-P1-C2_2		23.52		0.567		NA		9.55		-		2.72	
R2-SC-12-G-P1-C2_3		22.47		0.472		NA		7.26		-		2.60	
R2-SC-12-G-P1-C2_4		22.11		0.500		NA		7.76		-		2.55	
R4-HWSC-8-G-P2-C2_1	75.85	17.27	23.00	1.946	2.16	1.799	1.94	30.56	44.45	28.44	40.56	2.16	2.88
R4-HWSC-8-G-P2-C2_2		23.44		2.381		2.110		49.35		44.71		2.93	
R4-HWSC-8-G-P2-C2_3		24.68		2.072		1.840		45.36		41.33		3.09	
R4-HWSC-8-G-P2-C2_4		26.62		2.240		2.004		52.52		47.77		3.33	
R4-HWSC-14-G-P2-C2_1	75.85	16.93	20.43	2.252	1.67	NA	NA	34.76	26.94	1.14	0.88	2.12	2.56
R4-HWSC-14-G-P2-C2_2		21.01		2.453		NA		44.59		1.74		2.63	
R4-HWSC-14-G-P2-C2_3		20.92		0.814		NA		11.75		0.22		2.62	
R4-HWSC-14-G-P2-C2_4		22.84		1.171		NA		16.66		0.43		2.86	
R5-HWSC-14-H-P2-C2_1	75.85	25.96	26.98	0.289	0.46	0.043	0.15	4.87	9.32	0.96	2.78	3.25	3.38
R5-HWSC-14-H-P2-C2_2		27.04		0.497		0.245		10.47		5.87		3.38	
R5-HWSC-14-H-P2-C2_3		26.46		0.414		0.160		8.77		3.93		3.31	
R5-HWSC-14-H-P2-C2_4		28.45		0.621		NA		13.16		0.35		3.56	
R6-In-8-G-P3-C2_1	65.26	19.21	17.69	0.597	0.53	0.344	0.31	7.96	6.10	5.96	4.30	2.63	2.36
R6-In-8-G-P3-C2_2		19.39		0.474		0.263		6.19		4.25		2.66	
R6-In-8-G-P3-C2_3		14.08		0.591		0.312		5.94		3.59		1.93	
R6-In-8-G-P3-C2_4		18.10		0.464		0.335		6.18		5.07		2.48	
R6-In-12-G-P3-C2_1	66.93	18.23	18.40	0.542	0.39	0.263	0.23	8.51	6.33	4.32	3.87	2.46	2.48
R6-In-12-G-P3-C2_2		21.37		0.309		0.231		6.81		4.44		2.88	
R6-In-12-G-P3-C2_3		20.70		0.346		0.234		6.38		4.45		2.79	
R6-In-12-G-P3-C2_4		13.29		0.353		0.193		3.62		2.26		1.79	
R8-Rb-12-G-P4-C2_1	86.89	23.96	28.36	0.716	0.69	0.580	0.56	13.96	15.33	11.78	13.27	2.77	3.28
R8-Rb-12-G-P4-C2_2		30.95		0.724		0.494		16.35		12.43		3.58	
R8-Rb-12-G-P4-C2_3		28.04		0.473		0.437		10.04		10.24		3.24	
R8-Rb-12-G-P4-C2_4		30.50		0.841		0.724		20.97		18.65		3.52	
R9-Rb-12-G-P4-C2_1	67.56	18.23	18.09	2.344	1.94	2.116	1.75	35.26	28.84	33.11	27.13	2.45	2.43
R9-Rb-12-G-P4-C2_2		18.38		1.453		1.194		20.85		18.06		2.47	
R9-Rb-12-G-P4-C2_3		18.77		2.319		2.180		37.48		35.77		2.52	
R9-Rb-12-G-P4-C2_4		16.98		1.626		1.497		21.76		21.59		2.28	
R10-Rb-6-Steel-C2_1	65.26	21.73	20.04	1.319	1.09	0.955	0.59	25.18	19.88	18.681	10.61	2.98	2.75
R10-Rb-6-Steel-C2_2		14.13		0.573		0.323		5.35		3.660		1.94	
R10-Rb-6-Steel-C2_3		22.24		1.803		0.586		36.54		11.242		3.05	
R10-Rb-6-Steel-C2_4		22.05		0.664		0.476		12.47		8.854		3.02	

[a]Average value of nominally identical specimens; NA = not available.

Table 15
Experimental results for higher strength concrete mix – C2A (specimen symbols according to Fig. 6).

Specimen symbol	f_c (MPa)	$\tau_{b,max}$ (MPa)	$\tau_{b,max}$ [a] (MPa)	$s_{m,le}$ (mm)	$s_{m,le}$ [a] (mm)	$s_{m,fe}$ (mm)	$s_{m,fe}$ [a] (mm)	BE_{le} (Nmm)	BE_{le} [a] (Nmm)	BE_{fe} (Nmm)	BE_{fe} [a] (Nmm)	$\tau_{b,max}/f_{cm}^{0.5}$ ($MPa^{0.5}$)	$\tau_{b,max}/f_{cm}^{0.5}$ [a] ($MPa^{0.5}$)
R1-SC-12-C-P1-C2A_1	78.43	14.29	14.70	0.857	0.77	0.118	0.09	7.313	6.73	1.658	1.23	1.75	1.80
R1-SC-12-C-P1-C2A_2		14.31		0.825		0.102		7.454		1.350		1.76	
R1-SC-12-C-P1-C2A_3		16.31		0.553		0.036		4.975		0.518		2.00	
R1-SC-12-C-P1-C2A_4		13.89		0.854		0.106		7.193		1.394		1.70	
R2-SC-12-G-P1-C2A_1	78.43	21.94	21.81	0.310	0.34	0.088	0.09	5.360	5.74	1.854	0.68	2.69	2.68
R2-SC-12-G-P1-C2A_2		22.06		0.437		NA		7.001		0.289		2.71	
R2-SC-12-G-P1-C2A_3		21.84		0.306		NA		5.433		0.311		2.68	
R2-SC-12-G-P1-C2A_4		21.41		0.309		NA		5.160		0.281		2.63	
R4-HWSC-8-G-P2-C2A_1	65.19	20.20	22.42	0.281	0.44	0.082	0.09	3.738	6.00	1.529	1.79	2.77	3.07
R4-HWSC-8-G-P2-C2A_2		20.80		0.477		NA		6.298		-		2.85	
R4-HWSC-8-G-P2-C2A_3		24.22		0.571		NA		7.180		-		3.32	
R4-HWSC-8-G-P2-C2A_4		24.47		0.422		0.089		6.802		2.047		3.35	
R4-HWSC-14-G-P2-C2A_1	65.19	18.48	17.99	0.648	1.14	0.172	0.39	7.630	12.71	2.997	5.88	2.53	2.47
R4-HWSC-14-G-P2-C2A_2		19.47		0.936		0.218		11.416		3.986		2.67	
R4-HWSC-14-G-P2-C2A_3		19.10		1.483		0.230		14.962		4.093		2.62	
R4-HWSC-14-G-P2-C2A_4		14.90		1.510		0.930		16.828		12.442		2.04	
R5-HWSC-14-H-P2-C2A_1	78.43	32.41	31.57	NA	0.43	0.280	0.24	NA	10.86	8.251	6.93	3.98	3.87
R5-HWSC-14-H-P2-C2A_2		30.93		0.446		0.250		11.200		7.066		3.80	
R5-HWSC-14-H-P2-C2A_3		31.53		0.463		0.212		11.955		6.329		3.87	
R5-HWSC-14-H-P2-C2A_4		31.40		0.382		0.211		9.430		6.086		3.85	
R6-In-8-G-P3-C2A_1	65.19	14.71	13.39	0.642	0.39	0.225	0.22	3.690	3.62	2.696	2.47	2.02	1.78
R6-In-8-G-P3-C2A_2		11.83		0.190		0.100		1.665		0.958		1.62	
R6-In-8-G-P3-C2A_3		14.30		0.371		0.243		5.048		2.992		1.96	
R6-In-8-G-P3-C2A_4		12.73		0.378		0.314		4.144		3.451		1.75	
R6-In-12-G-P3-C2A_1	75.22	17.78	17.82	0.777	0.81	0.269	0.29	9.427	10.29	4.253	4.72	2.24	2.24
R6-In-12-G-P3-C2A_2		17.61		0.776		0.314		9.826		5.081		2.22	
R6-In-12-G-P3-C2A_3		16.49		0.821		0.285		10.154		4.235		2.07	
R6-In-12-G-P3-C2A_4		19.39		0.849		0.301		11.743		5.314		2.44	
R8-Rb-12-G-P4-C2A_1	65.19	17.98	18.47	2.183	1.87	1.706	1.60	32.634	29.05	27.012	26.53	2.47	2.53
R8-Rb-12-G-P4-C2A_2		19.35		1.668		1.543		27.110		26.506		2.65	
R8-Rb-12-G-P4-C2A_3		20.26		1.731		1.599		29.938		29.539		2.78	
R8-Rb-12-G-P4-C2A_4		16.27		1.910		1.535		26.526		23.069		2.23	
R9-Rb-12-G-P4-C2A_1	75.22	20.84	19.39	1.543	1.48	0.959	1.02	24.295	21.42	16.861	16.28	2.62	2.44
R9-Rb-12-G-P4-C2A_2		19.51		1.697		1.146		23.615		18.207		2.45	
R9-Rb-12-G-P4-C2A_3		18.61		1.068		0.706		14.038		10.405		2.34	
R9-Rb-12-G-P4-C2A_4		18.59		1.623		1.274		23.735		19.642		2.34	

[a]Average value of nominally identical specimens; NA = not available.

References

[1] Bertolini L, Elsener B, Pedeferri P, Redaelli E, Polder RB. Corrosion of Steel in Concrete: Prevention, Diagnosis, Repair. Second Edi. Weinheim, Germany: Wiley-VCH; 2014.

[2] Nanni A, De Luca A, Zadeh H. Reinforced Concrete with FRP Bars. Boca Raton, FL: CRC Press - Taylor & Francis Group; 2014. doi:10.1201/b16669.

[3] K. Pilakoutas, K. Neocleous, M. Guadagnini, Design philosophy issues of fiber reinforced polymer reinforced concrete structures, J. Compos. Constr. 6 (2002) 154–161.

[4] Balázs GL, Borosnyói A. Long-term behavior of FRP. ASCE Proc. Int. Work. Compos. Constr. A Real., Capri, Italy: 20-21 July 2001; 2001, p. 84–91.

[5] L. Du, K.J. Folliard, Mechanisms of air entrainment in concrete, Cem. Concr. Res. 35 (8) (2005) 1463–1471, https://doi.org/10.1016/j.cemconres.2004.07.026.

[6] M. Barfield, N. Ghafoori, Air-entrained self-consolidating concrete: A study of admixture sources, Constr. Build. Mater. 26 (1) (2012) 490–496, https://doi.org/10.1016/j.conbuildmat.2011.06.049.

[7] J. Schock, S. Liebl, K. Achterhold, F. Pfeiffer, Obtaining the spacing factor of microporous concrete using high-resolution Dual Energy X-ray Micro CT, Cem. Concr. Res. 89 (2016) 200–205, https://doi.org/10.1016/j.cemconres.2016.08.008.

[8] A.I. El Mir, Influence of additives on the porosity related properties of self-compacting concrete, PhD thesis, Budapest University of Technology and Economics, 2017.

[9] L.J. Struble, Q. Jiang, Effects of Air Entrainment on Rheology, ACI Mater. J. 101 (2004) 448–456, https://doi.org/10.1061/(ASCE)0733-9429(1991)117:2(262).

[10] B. Łaźniewska-Piekarczyk, The type of air-entraining and viscosity modifying admixtures and porosity and frost durability of high performance self-compacting concrete, Constr. Build. Mater. 40 (2013) 659–671, https://doi.org/10.1016/j.conbuildmat.2012.11.032.

[11] M. Baena, L. Torres, A. Turon, C. Barris, Experimental study of bond behaviour between concrete and FRP bars using a pull-out test, Compos. Part B Eng. 40 (8) (2009) 784–797, https://doi.org/10.1016/j.compositesb.2009.07.003.

[12] Sólyom S, Di Benedetti M, Balázs GL. Effect of surface characteristics of FRP bars on bond behavior in concrete. ACI SP 2018;327:41.1-41.20.

[13] S. Sólyom, G.L. Balázs, Influence of FRC on bond characteristics of FRP reinforcement, in: K. Maekawa, A. Kasuga, J. Yamazaki (Eds.), 11th fib Int, PhD Symp. Civ. Eng, Tokyo, Japan, 2016, pp. 271–278.

[14] A. Veljkovic, V. Carvelli, M.M. Haffke, M. Pahn, Concrete cover effect on the bond of GFRP bar and concrete under static loading, Compos. Part B Eng. 124 (2017) 40–53, https://doi.org/10.1016/j.compositesb.2017.05.054.

[15] F. Sayed Ahmad, G. Foret, R. Le Roy, Bond between carbon fibre-reinforced polymer (CFRP) bars and ultra high performance fibre reinforced concrete (UHPFRC): Experimental study, Constr. Build. Mater. 25 (2) (2011) 479–485, https://doi.org/10.1016/j.conbuildmat.2010.02.006.

[16] M. Antonietta Aiello, M. Leone, M. Pecce, Bond Performances of FRP Rebars-Reinforced Concrete, J. Mater. Civ. Eng. 19 (3) (2007) 205–213.

[17] Solyom S, Balázs GL. Bond of FRP bars with different surface characteristics. Constr. Build. Mater. 2020;264. doi:10.1016/j.conbuildmat.2020.119839.

[18] Guadagnini M, Pilakoutas K, Waldron P, Achillides Z. Tests for the evaluation of bond properties of FRP bars in concrete. In: Seracino R, Balkema AA, editors. 2nd Int. Conf. FRP Compos. Civ. Eng. (CICE 2004), Adelaide: 2004, p. 343–50.

[19] N. Saleh, A. Ashour, D. Lam, T. Sheehan, Experimental investigation of bond behaviour of two common GFRP bar types in high – Strength concrete, Constr. Build. Mater. 201 (2019) 610–622, https://doi.org/10.1016/j.conbuildmat.2018.12.175.

[20] Basaran B, Kalkan I. Investigation on variables affecting bond strength between FRP reinforcing bar and concrete by modified hinged beam tests. Compos. Struct. 2020;242. doi:10.1016/j.compstruct.2020.112185.

[21] E. Cosenza, G. Manfredi, R. Realfonzo, Behavior and Modeling of Bond of FRP Rebars to Concrete, J. Compos. Constr. 1 (2) (1997) 40–51, https://doi.org/10.1061/(ASCE)1090-0268(1997)1:2(40).

[22] M. Rezazadeh, V. Carvelli, A. Veljkovic, Modelling bond of GFRP rebar and concrete, Constr. Build. Mater. 153 (2017) 102–116, https://doi.org/10.1016/j.conbuildmat.2017.07.092.

[23] S. Islam, H.M. Afefy, K. Sennah, H. Azimi, Bond characteristics of straight- and headed-end, ribbed-surface, GFRP bars embedded in high-strength concrete, Constr. Build. Mater. 83 (2015) 283–298, https://doi.org/10.1016/j.conbuildmat.2015.03.025.

[24] F. Yan, Z. Lin, D. Zhang, Z. Gao, M. Li, Experimental study on bond durability of glass fiber reinforced polymer bars in concrete exposed to harsh environmental agents: Freeze-thaw cycles and alkaline-saline solution, Compos. Part B Eng. 116 (2017) 406–421, https://doi.org/10.1016/j.compositesb.2016.10.083.

[25] Solyom S, Di Benedetti M, Guadagnini M, Balázs GL. Effect of temperature on the bond behaviour of GFRP bars in concrete. Compos. Part B Eng. 2020;183. doi: 10.1016/j.compositesb.2019.107602.
[26] Sólyom S, Balázs GL, Di Benedetti M, Guadagnini M, Zappa E. Bond Strength of GFRP Rebars In Concrete at Elevated Temperature. In: Guadagnini M, Keighley S, editors. Adv. Compos. Constr. ACIC 2017 - Proc. 8th Bienn. Conf. Adv. Compos. Constr., Sheffield, UK: 2017, p. 337–43.
[27] É. Lublóy, V. Hlavicka, Bond after fire, Constr. Build. Mater. 132 (2017) 210–218, https://doi.org/10.1016/j.conbuildmat.2016.11.131.
[28] T. D'Antino, M.A. Pisani, Influence of sustained stress on the durability of glass FRP reinforcing bars, Constr. Build. Mater. 187 (2018) 474–486, https://doi.org/10.1016/j.conbuildmat.2018.07.175.
[29] Benmokrane B, Brown VL, Mohamed K, Nanni A, Rossini M, Shield C. Creep-Rupture Limit for GFRP Bars Subjected to Sustained Loads. J. Compos. Constr. 2019;23. doi:10.1061/(asce)cc.1943-5614.0000971.
[30] M. Pecce, G. Manfredi, R. Realfonzo, E. Cosenza, Experimental and analytical evaluation of bond properties of GFRP bars, J. Mater. Civ. Eng. 13 (4) (2001) 282–290.
[31] E. Gudonis, R. Kacianauskas, V. Gribniak, A. Weber, R. Jakubovskis, G. Kaklauskas, Mechanical Properties of the Bond Between GFRP Reinforcing Bars and Concrete, Mech. Compos. Mater. 50 (4) (2014) 457–466, https://doi.org/10.1007/s11029-014-9432-0.
[32] Siess EH and CP. Effect of Entrained Air on Bond Between Concrete and Reinforcing Steel. ACI J. Proc. 1950;46. doi:10.14359/12085.
[33] S. Huaishuai, W. Zhiheng, Z. Peng, Z. Tiejun, F. Guoxi, R. Guosheng, Bond behavior of steel bar in air-entrained RCAC in fresh water and sea water after fast freeze-thaw cycles, Cold Reg. Sci. Technol. 135 (2017) 90–96, https://doi.org/10.1016/j.coldregions.2016.11.005.
[34] e-UT 07.01.14. Design guidelines for road bridges: IV. Concrete, reinforced concrete and prestressed road bridges (In Hungarian: Közúti hidak tervezési előírásai IV. Beton, vasbeton és feszített vasbeton közúti hidak tervezése). 2004.
[35] Hao Q, Wang Y, Ou J. Development Length of Glass Fiber Reinforced Plastic (GFRP)/ Steel Wire Composite Rebar. CICE 2010 - 5th Int. Conf. FRP Compos. Civ. Eng., Beijing, China: 2010, p. 1–4.
[36] Simtrec Canada, Prestressing Concrete Structures with Fibre Reinforced Polymers, Calgary, Alberta, 2007.
[37] B.W. Wambeke, C.K. Shield, Development length of glass fiber-reinforced polymer bars in concrete, ACI Struct. J. 103 (2006) 11–17.
[38] S.M. Pour, M.S. Alam, A.S. Milani, Improved bond equations for Fiber-Reinforced Polymer bars in concrete, Materials (Basel) 9 (2016) 1–14, https://doi.org/10.3390/ma9090737.
[39] C.E. Bakis, A. Nanni, J.A. Terosky, S.W. Koehler, Self-monitoring, pseudo-ductile, hybrid FRP reinforcement rods for concrete applications, Compos. Sci. Technol. 61 (6) (2001) 815–823, https://doi.org/10.1016/S0266-3538(00)00184-6.
[40] EN 12350-5. Testing fresh concrete. Part 5: Flow table test, 2009.
[41] EN 12390-3. Testing hardened concrete. Part 3: Compressive strength of test specimens, 2009.
[42] EN 480-11. Admixtures for concrete, mortat and grout - Test ethods - Part 1: Determination of air void characteristics in hardened concrete. European Committee for Standardization; 2005.
[43] B. Łaźniewska-Piekarczyk, The influence of admixtures type on the air-voids parameters of non-air-entrained and air-entrained high performance SCC, Constr. Build. Mater. 41 (2013) 109–124, https://doi.org/10.1016/j.conbuildmat.2012.11.086.
[44] ACI 201.2R-08. Guide to Durable Concrete. Farmington Hills, MI: American Concrete Institute (ACI); 2008.
[45] N.P. Mayercsik, R. Felice, M.T. Ley, K.E. Kurtis, A probabilistic technique for entrained air void analysis in hardened concrete, Cem. Concr. Res. 59 (2014) 16–23, https://doi.org/10.1016/j.cemconres.2014.01.023.
[46] R. Tepfers, L. De Lorenzis, Bond of FRP reinforcement in concrete — A challenge, Mech. Compos. Mater. 39 (2003) 477–497.
[47] RILEM, RC6: Bond test for reinforcement steel. 2. Pull-out test, Mater. Struct. 6 (1983) 218–221.
[48] ACI Committee 440. ACI 440.3R-04: Guide test methods for Fiber-Reinforced Polymers (FRPs) for reinforcing or strengthening concrete structures. Farmington Hills, MI: 2004.
[49] CSA-S806-12. Design and construction of building structures with fibre-reinforced polymers. Mississauga, Ontario, Canada: Canadian Standards Association; 2012.
[50] fib. International Federation for Structural Concrete – Model Code for Concrete Structures 2010. Ernst & Sohn; 2013.
[51] S. Solyom, M. Di Benedetti, A. Szijártó, G.L. Balázs, Non-metallic reinforcements with different moduli of elasticity and surfaces for concrete structures, Architect. Civil Eng. Environ. 11 (2018) 79–88, https://doi.org/10.21307/ACEE-2018-025.
[52] D.J. Sheskin, Handbook of Parametric and Nonparametric Statistical Procedures. Fifth Edit, Chapman & Hall book, CRC Press, Boca Raton, FL, 2011.
[53] Lu Z, Yuan K-H. Welch's t test. In: Salkind NJ, editor. Encycl. Res. Des., Thousand Oaks; 2010, p. 1620–3. doi:10.13140/RG.2.1.3057.9607.
[54] IBM Corp. IBM SPSS Statistics for Windows, Version 26.0. 2019.
[55] Laerd Statistics. Independent-samples t-test using SPSS Statistics. Statistical tutorials and software guides 2015:Retrieved from https://statistics.laerd.com/.
[56] Montgomery DC, Runger GC. Applied Statistics and Probability for Engineers. Fifth Edit. John Wiley & Sons, Inc.; 2010.
[57] Japanese Society of Civil Engineers (JSCE). Recommendations for design and construction for concrete structures using continuous fibre reinforcing materials. Concr. Eng. Ser. 1997.
[58] CAN/CSA-S6-06. Canadian Highway Bridge Design Code. Mississauga, Ontario, Canada: 2006.
[59] D.G. Altman, Practical Statistics for Medical Research, Taylor & Francis, 1990.